Synthesis and stability of [^{45}Ti]Ti-DOTA complex: en route towards aza-macrocyclic ^{45}Ti-based radiopharmaceuticals

Tamal Roy,[a] Eduard Pogorilyy,[a] Chubina P. Kumarananthan,[b] Unni A. Kvitastein,[b] Marco Foscato,[a] Karl W. Törnroos,[a] Tom C. H. Adamsen,*[a,b] Erwan Le Roux*[a]

[a.] University of Bergen, Department of Chemistry, Allégaten 41, Bergen, Norway.
[b.] Centre for Nuclear Medicine and 180 °N - Bergen Tracer Development Centre, Department of Radiology, Haukeland University Hospital, Bergen, Norway.

Table of Content:

Abbreviations:

DOTA = 1,4,7,10-tetraazacyclododecane-1,4,7,10-tetraacetic acid
salan = *N*,*N*′-bis-(salicylidene)ethylenediamine)
DFO = deferoxamine
LDFC = linear desferrichrome
THP = tris(hydroxypyridinone)
TREN = tris(2-aminoethyl)amine
CAM = catecholamide
EDTA = 2,2′,2″,2‴-(ethane-1,2-diyldinitrilo)tetraacetic acid
PSMA = prostate specific membrane antigen
DUPA = 2-[3-(1,3-dicarboxypropyl)ureido]pentanedioic acid

General Methods and Materials

Unless state otherwise, all experiments were carried out in oven dried glassware. Majority of the chemicals, solvents, and NMR solvents such as D_2O and dmso-d_6 were purchased from Sigma-Aldrich. $Sc(NO_3)_3$ hydrate (99.999% trace metal basis) was received from REacton, triethylamine (≥ 99.0%, suitable for synthesis), ultrapure nitric acid (60%) and ultrapure water were obtained from Merck. Guaiacol (>99%) and anisole (99%, pure) were received from Acros Organics. DMSO (≥ 99.9%), pyridine (99.8 %, anhydrous), acetonitrile (gradient grade for liquid chromatography) and TFA (≥ 99.0 %, suitable for HPLC) was supplied by SUPELCO. DOTA, 1,4,7,10-Tetraazacyclododecane-1,4,7,10-tetraacetic acid (97%) was supplied from abcr and was used as it is without further purifications. Metal precursors ($MgSO_4$, $FeCl_3.6H_2O$, $CoCl_2$, $CuSO_4.5H_2O$, $ZnCl_2$,), and $M(OiPr)_4.xHOiPr$ (with M = Ti with x = 0, and M = Zr and Hf with x = 1) precursor and $TiCl_4$ were obtained from Sigma-Aldrich, and used as received. The NMR spectra of compounds were recorded by using NMR tubes at 25±1 °C on a *Bruker*-BIOSPIN-AV500 (5 mm BBO, ^{1}H: 500.13 MHz; ^{13}C: 125.77 MHz) and a Bruker BioSpin AVANCE III HD 850 MHz (5mm TCI CryoProbe, ^{1}H: 850.13 MHz; ^{13}C: 213.77 MHz). ^{1}H and ^{13}C shifts are referenced to internal solvent resonances and reported in ppm relative to TMS. HR-MS(ESI) analysis was performed on JEOL AccuTOF^{TM} JMS T100 LC mass spectrometer using positive ionization mode. HPLC analysis was performed on Agilent 1260 Infinity II using Agilent Poroshell 120 EC-C18 (4 µm, 4.6 mm × 100 mm) column (conditions used: a flow rate of 1 mL/min, mobile phase of 0 to 70% of acetonitrile in water, runtime 20 min, 0.1% of TFA buffer, 254 nm wavelength used in UV detection). DRIFT spectra were obtained by using a Nicolet protégé 460 ESP FTIR spectrometer and a DRIFT cell (equipped with KBr windows). The spectra were averaged over 64 scans; the resolution was ±4 cm^{-1}. Elemental analyses were performed by Mikroanalytisches Labor Pascher.

The productions of ^{45}Ti were performed in a GE PETtrace 860 cyclotron equipped with a GE PETtrace 800 ^{68}Ga Liquid target (Haukeland University Hospital, Bergen, Norway). A proton energy of 14.3 MeV was achieved with the use of an aluminium degrader foil (200 µm). The liquid target was also equipped with a Havar foil (25 µm) and niobium foil (25 µm). The activity and radionuclidic purity of the cyclotron products and other samples were measured in a Canberra high-purity germanium detector (model: GC3018, detector diameter: 60.8 mm, detector length: 46.5 mm). The detector was run with Apex-gamma (V1.1.4)/ Genie 2000 (3.4) software. The cyclotron products were cooled down for 40 – 105 min after EOB to let shorter lived radionuclides, such as hazardous gaseous species containing ^{13}N and ^{11}C decay. These positron emitters are produced when irradiating aqueous targets through the $^{16}O(p,\alpha)^{13}N$ reaction and nitric acid through the $^{14}N(p,\alpha)^{11}C$.[1] The initial activity (t = 0) for determining the extraction efficiency (EE) and the radiochemical yield (RCY) were taken after the cooling period. All samples were either measured 0 or 11.7 cm from the detector for either 10 or 20 min. The radiochemical reaction progress and purity were analysed with an analytical radio-HPLC (Agilent 1260, Infinity instrument) that was run with a Laura software (version 4.1.14.96 SP1). The radio-HPLC was attached to a Posi-RAM radio-HPLC detector (model 4, LabLogic) and Acclaim® 120 C18 Bonded Silica column (5 µm, 120 Å, 4.6 x 250 mm, Dionex). The Ti-DOTA complexes were analysed at 254 nm using a mobile phase consisting of 0.1% TFA/MeCN (solvent A) and 0.1 % TFA/H_2O (solvent B). A gradient method was used where solvent A was at 5 % from 0 to 3 min, increased to 35% after 10 min, further increased to 75% after 15 min, and finally decreased to 5 % after 20 min.

Computational Details

Initial molecular geometries of DOTA complexes were created by manually adapting the crystallographic geometries of Zn and Bi taken from The Cambridge Structure Database, ref codes UCITOS and HADRAG. The initial geometries for water clusters were inspired by the work of Maheshwary. [2] All subsequent molecular modelling was performed with Gaussian16-C.01.[3]

Geometry Optimization. Geometry optimizations were performed in DFT (Density functional theory) using the generalized gradient approximation (GGA) functional by Perdew, Burke and Ernzerhof (PBE)[4, 5] in conjunction with Grimme's D3 empirical dispersion term[6] with revised Becke-Johnson damping (GD3MBJ).[7] Interaction with solvent (water) was accounted for by including in the all parts of the DFT protocol the SMD version of the corresponding polarizable continuum model.[8] The overall DFT model is named PBE-GD3MBJ-SMD(water), for brevity. All carbon and hydrogen atoms were described by the def2-TZVP[9] basis set obtained from the basis set exchange (BSE) website,[10, 11] while oxygen and nitrogen by def2-TZVPD[9, 12] from the BSE website. While titanium atoms was described by the def2-TZVP[9] basis set from BSE, zirconium and hafnium atoms were described by the def2-TZVP[9] basis set taken from BSE coupled with the relativistic effective core potential (ECP*n*MDF)[13, 14] obtained from the Stuttgart/Cologne Group website.[15] Prior to the geometry optimization the electronic state was checked for internal instabilities and possibly re-optimized to the real, restricted solution. Gaussian16's ultrafine integration grid was used throughout the protocol, and Gaussian16's fine grid was used for Coupled Perturbed Hartree-Fock (CPHF). The self-consistent field (SCF) procedure performed during geometry optimization was considered converged when the RMS change in density matrix was lower than $1.0 \cdot 10^{-9}$ and the maximum change in density matrix lower than $1.0 \cdot 10^{-7}$. The geometry optimization was converged to tight convergence criteria (max. force $1.5 \cdot 10^{-5}$ a.u., RMS force $1.0 \cdot 10^{-5}$ a.u., max. displacement $6.0 \cdot 10^{-5}$ a.u., RMS displacement $4.0 \cdot 10^{-5}$ a.u.), without symmetry constraints. The nature of the optimized stationary points was determined by the analysis of the eigenvalues of the analytical Hessian computed at the stationary point to confirm that all minima had no imaginary mode. The translational, rotational, and vibrational corrections to the Gibbs free energies were calculated within the ideal-gas, rigid-rotor, and harmonic oscillator approximations (298 K), but all frequencies below 100 cm^{-1} were shifted to 100 cm^{-1} when calculating the vibrational component of the entropy (i.e., quasi-harmonic oscillator approximation).[16]
Energies (E^{TZ}) and thermal correction (G_{qh}^{298K}) for all molecular models are reported in Table S2. The input files and the results of the geometry optimizations and Hessian calculations are available in the ioChem-BD[17, 18] repository at https://doi.org/10.19061/iochem-bd-6-344.

Single Point Energies. Final single point energy calculations were performed with the DFT model described above, *i.e.*, PBE-GD3MBJ-SMD(water), but using basis sets with overall quadruple-ζ quality. Namely, while nitrogen and oxygen were described by the def2-QZVPD[9, 12] from BSE, and carbon, hydrogen, and titanium atoms by def2-QZVP[19] from BSE, for zirconium and hafnium the def2-QZVP[19, 20] basis set taken from BSE was coupled with the ECP*n*MDF[13, 14] obtained from the Stuttgart/Cologne Group website.[15] The ultrafine integration grid was used throughout the protocol. The self-consistent field (SCF) procedure performed did not consider symmetry constraints and converged until the RMS change in density matrix was lower than $1.0 \cdot 10^{-5}$ and the maximum change in density matrix lower than $1.0 \cdot 10^{-3}$.

Energies (E^{QZ}) for all molecular models are reported in Table S2. The input files and the parsed results are available in the ioChem-BD repository[17, 18] at https://doi.org/10.19061/iochem-bd-6-344.

Calculation of Free Energies. Gibbs free energies were calculated at 298 K according to:

$$G_{\square}^{298K\,[1M]} = E_{\square}^{QZ} + G_{qh}^{298K} + G_{1atm\rightarrow 1M}^{298K}$$

where E^{QZ} is the potential energy resulting from single-point calculation; G_{qh}^{298K} is the thermal correction to the Gibbs free energy calculated at the geometry optimization level with the quasi-harmonic approximation at 298 K; and $G_{1atm\rightarrow 1M}^{298K}$ is the correction of the standard state from 1 atm to 1 M solution exhibiting infinite-dilution, ideal-gas-like behaviour, which is equal to 1.89 kcal mol^{-1} (= RT·ln(24.46)) at room temperature. All computed values are reported in Table S2.

Synthesis Details

Synthesis of DOTA chelator. The synthesis of 1,4,7,10 tetraazacyclododecane-1,4,7,10-tetraacetic acid (DOTA) was adapted from a slightly modified procedure.[21] Cyclen (5.25 g, 30.5 mmol), lithium hydroxide monohydrate (10.68 g, 254.5 mmol) and water (30 mL) were introduced into a round bottom flask (500 mL) and cooled to at 5-10 °C. Then, a solution of bromoacetic acid (17.70 g, 127.4 mmol) in water (12 mL) was added to this solution while maintaining the temperature between 5-10 °C. The resulting mixture was allowed to warm to room temperature and stirred for 24 h. To the reaction mixture, 37% hydrochloric acid (13 mL) and ethanol (200 mL) were added leading to a precipitate, and then followed by filtration. The resulting solid was dried for 6 h under reduced pressure at 120 °C. Yield: 86% (13.45 g, 26.2 mmol). ^{1}H NMR (500.13 MHz, D_2O) δ 3.76 (s, 8H), 3.28 (s, 16H) ppm; ^{13}C NMR (125.77 MHz, D_2O, 298 K) δ 172.81, 54.91, 49.47 ppm. IR (KBr): 2990, 2502, 1742, 1383, 1192, 918, 779 cm^{-1}. HR-MS (ESI): Calculated for $C_{16}H_{29}N_4O_8$, 405.19854 [(M+H)$^+$] Found: 405.19802 [(M+H)$^+$].

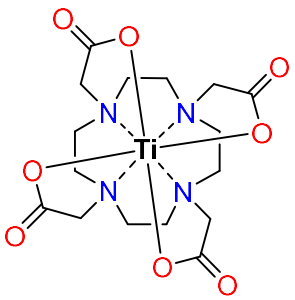

Representative procedure for the synthesis of Ti-DOTA. To a degassed solution of DOTA (0.40 g, 1.0 mmol) in MeOH (10 mL) was added Ti(O*i*Pr)$_4$ (0.28 g, 1.0 mmol), and the resulting solution was allowed to react at 70 °C for 16 h. Next, the resulting suspension was filtered. The precipitate thus obtained was washed with MeOH (2 x 5 mL) and water (2 x 5 mL), and air dried in an oven to give Ti-DOTA as a white solid: Yield: 89% (0.40 g, 0.89 mmol). ^{1}H NMR (850.13 MHz, D_2O): δ 4.43 (d, J = 18.0 Hz, 4H), 4.09 (d, J = 18.0 Hz, 4H), 3.69 (td, J = 14.1, 4.1 Hz, 4H), 3.41 (dd, J = 14.3, 3.9 Hz, 4H), 3.34 (td, J = 14.1, 3.5 Hz, 4H), 3.10 (dd, J = 14.3, 3.3 Hz, 4H) ppm. ^{13}C NMR (213.76 MHz, D_2O): δ 180.1, 69.7, 59.3, 58.2 ppm. DRIFT (KBr): ν 2937, 1679, 1479, 1464, 1425, 1398, 1364, 1329, 1295, 1268, 1242, 1160, 1079, 1079, 1035, 997, 939 cm^{-1}. HR-MS (ESI): calcd. for $C_{16}H_{25}N_4O_8Ti$ [M+H]$^+$: 449.1152, found: 449.1149. Anal. Calcd. for $C_{16}H_{24}N_4O_8Ti$: C, 42.87; H, 5.40; N, 12.50; Ti, 10.68%. Found: C, 42.55; H, 5.42; N, 12.4; Ti, 11.0%.

Note: Ti-DOTA is soluble in boiling water, and the ^{1}H NMR spectroscopy of the solids obtained after cooling down, remains identical to the initial ^{1}H NMR spectrum.

Table S1: Reaction conditions for the synthesis of Ti-DOTA.

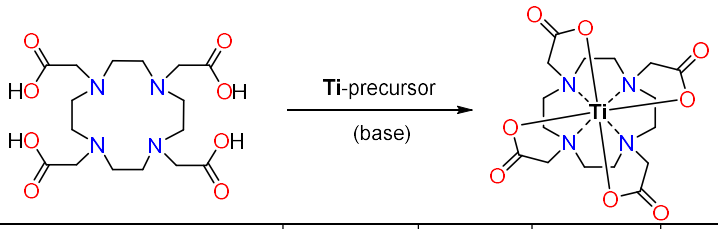

Entry	Ti Precursor	Solvent	Temp. (°C)	Base (equiv.)	Time (h)	Yield (%)[a]
1	$Ti(OiPr)_4$	toluene	70	-	24	67
2	$Ti(OiPr)_4$	MeCN	70	-	24	69
3	$Ti(OiPr)_4$	EtOH	70	-	24	73
4	$Ti(OiPr)_4$	MeOH	70	-	16	89
5	$TiCl_4$[b]	MeOH	60	NEt_3 (5)	16	27
6	$[NH_4]_2[Ti(CH_3CH(O)CO_2)(OH)_2]$	water	100	-	24	2

[a] Isolated yield. [b] 1 M in toluene.

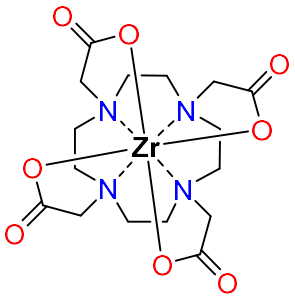

Synthesis of Zr-DOTA. The synthesis procedure was adapted and modified from Pandya et al.[22] To a degassed solution of DOTA (0.40 g, 1.0 mmol) in MeOH (10 mL) was added $Zr(OiPr)_4.HOiPr$ (0.39 g, 1.0 mmol), and the resulting solution was allowed to react at 70 °C for 24 h. Next, the resulting suspension was filtered. The precipitate thus obtained was washed with MeOH (2 x 10 mL) and water (2 x 5 mL), and air dried in an oven to give Zr-DOTA as a white solid: Yield: 88% (0.43 g, 0.88 mmol). ^{1}H NMR (500.13 MHz, D_2O): δ 4.06 (d, J = 17.4 Hz, 4H), 3.74 (d, J = 17.3 Hz, 4H), 3.63 (td, J = 14.2, 3.6 Hz, 4H), 3.20 (dd, J = 14.4, 3.6 Hz, 4H), 3.06 (td, J = 14.2, 3.6 Hz, 4H), 2.93 (dd, J = 14.7, 3.3 Hz, 4H) ppm. ^{13}C NMR (125.77 MHz, D_2O): δ 179.3, 67.4, 56.7, 56.6 ppm. DRIFT (KBr): ν 2994, 1682, 1464, 1299, 1073, 934 cm^{-1}. HR-MS (ESI): calcd. for $C_{16}H_{25}N_4O_8Zr$ $[M+H]^+$: 491.0719, found: 491.0712.

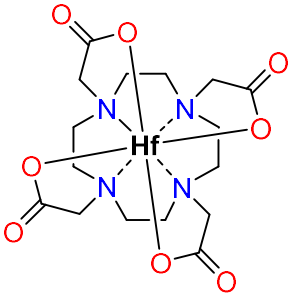

Synthesis of Hf-DOTA. To a degassed solution of DOTA (0.404 g, 1.0 mmol) in MeOH (10 mL) was added $Hf(OiPr)_4.HOiPr$ (0.415 g, 1.0 mmol), and the resulting solution was allowed to react at 70 °C for 96 h. Next, the resulting suspension was filtered. The precipitate thus obtained was washed with MeOH (2 x 10 mL) and water (2 x 5 mL), and air dried in an oven to give Hf-DOTA as a white solid: Yield: 25% (0.142 g, 0.25 mmol). ^{1}H NMR (850.13 MHz, D_2O) δ 4.15 (d, J = 17.8 Hz, 4H), 4.01 (d, J = 17.8 Hz, 4H), 3.63 (td, J = 14.5, 3.7 Hz, 4H), 3.42 (dd, J = 14.5, 3.6 Hz, 4H), 3.14 (td, J = 14.2, 3.6 Hz, 4H), 3.09 (dd, J = 14.6, 3.5 Hz, 4H) ppm. ^{13}C NMR (213.76 MHz, D_2O): δ 179.1, 67.7, 57.0, 56.5 ppm. DRIFT (KBr): ν 2995, 1685, 1302, 1073, 935, 806 cm^{-1}. HR-MS (ESI): calcd. for $C_{16}H_{25}N_4O_8Hf$ $[M+H]^+$: 581.1138, found: 581.1136.

Characterization Data for M-DOTA Complexes

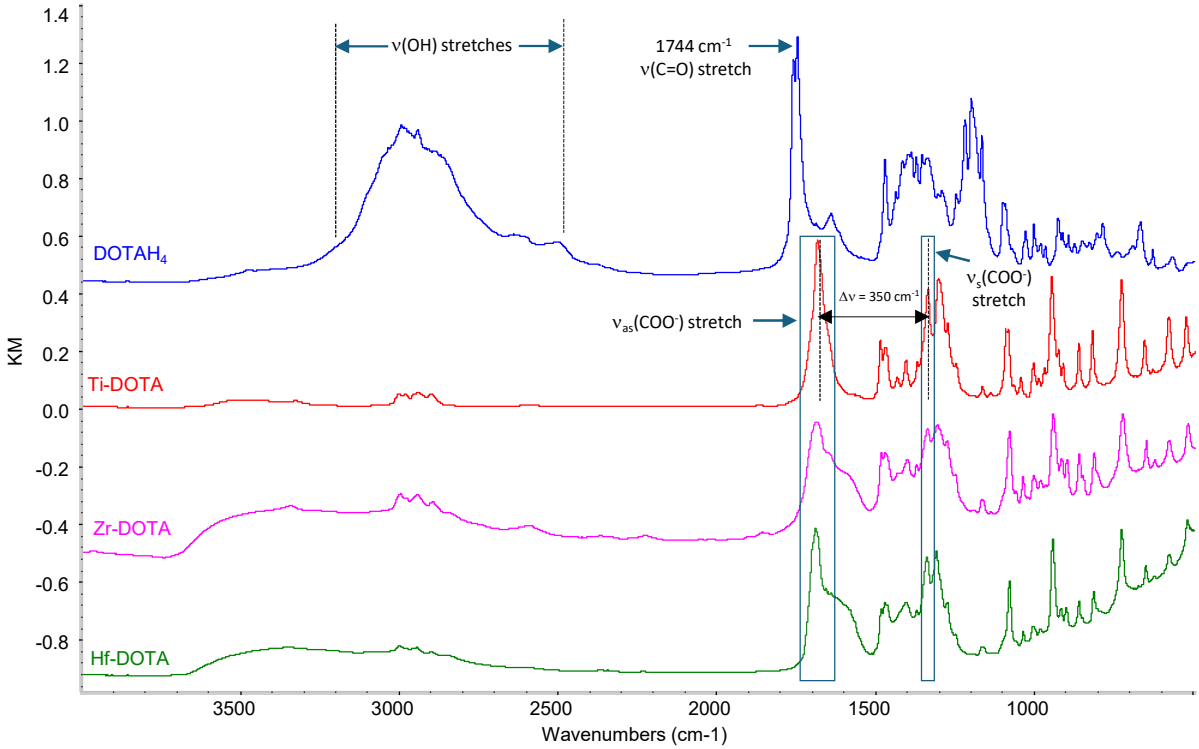

Figure S1. DRIFT spectra of free DOTA chelator (in blue) and M-DOTA complexes (Ti-DOTA in red, Zr-DOTA in pink, and Hf-DOTA in green).

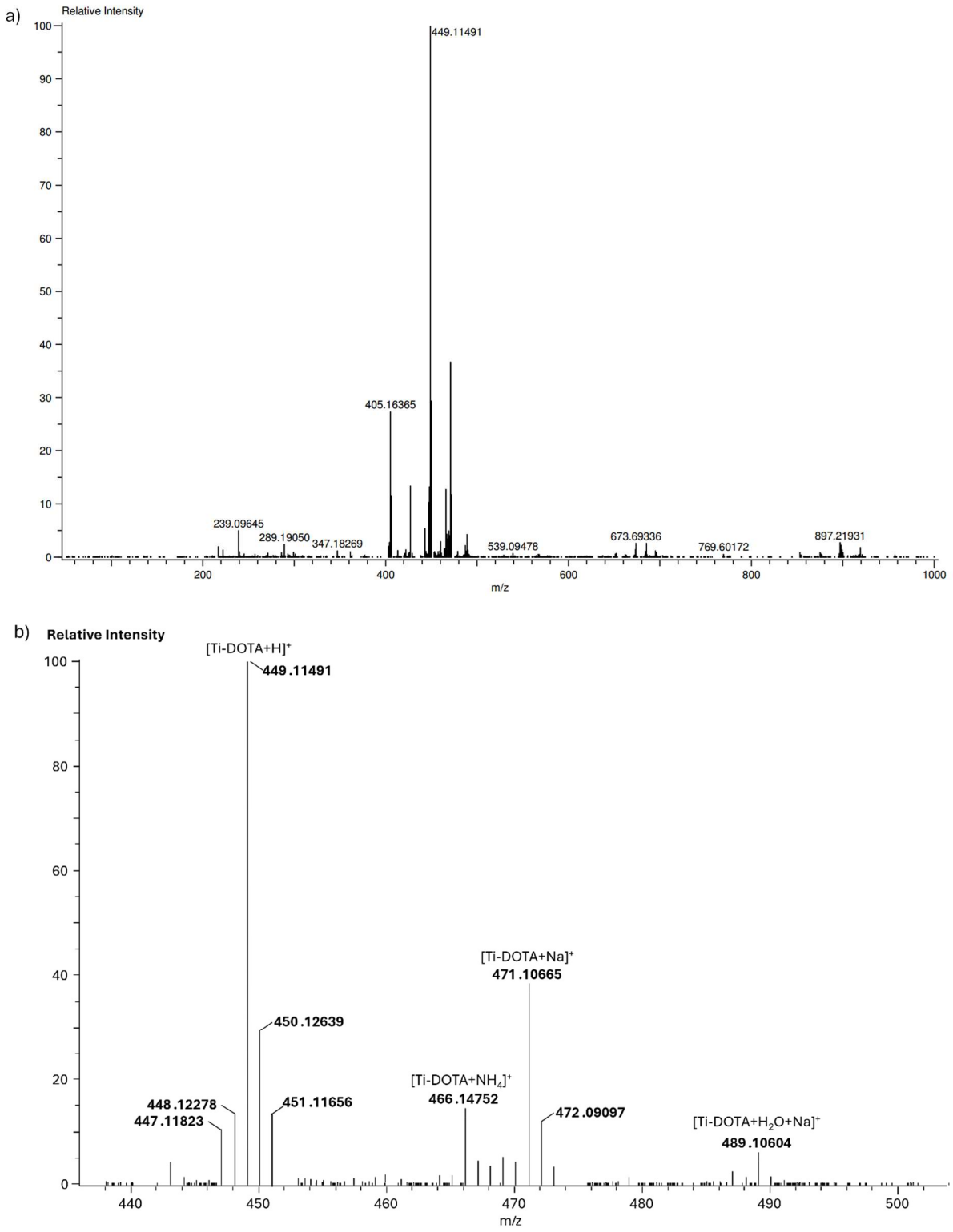

Figures S2. HR-MS (ESI^+) spectra of Ti-DOTA: a) full spectrum, and b) expanded region near the base peak at 449.11491 m/z.

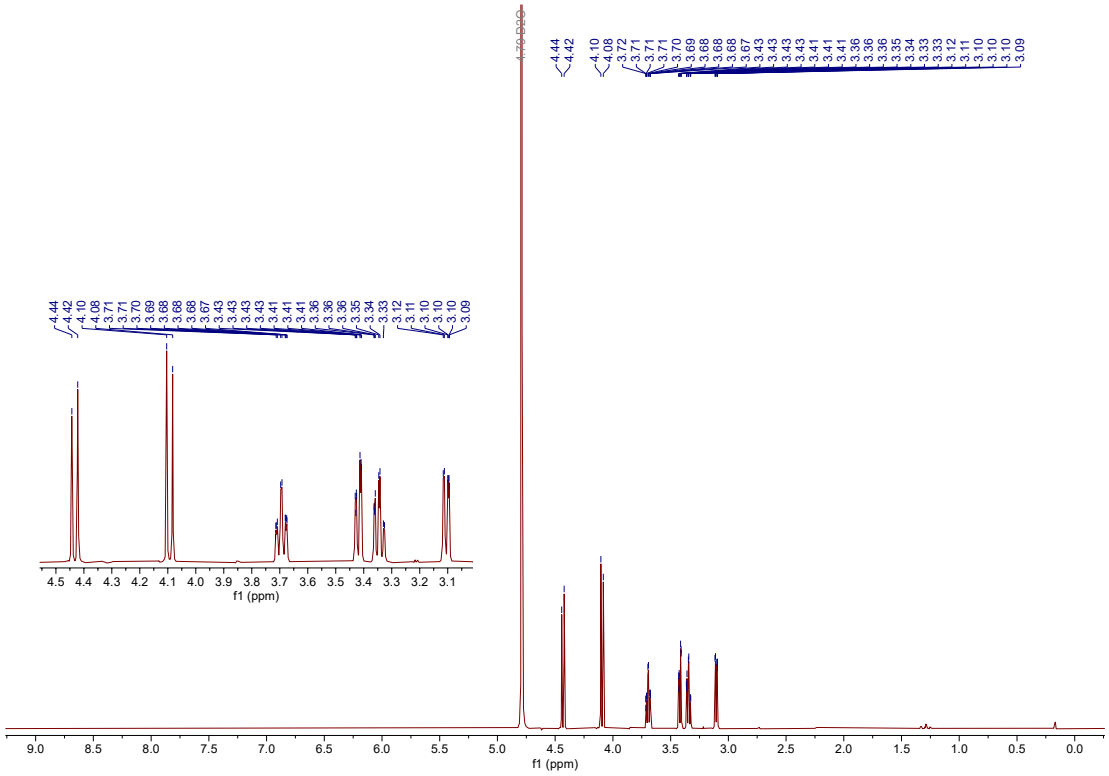

Figure S3. ^{1}H NMR spectrum of Ti-DOTA in D_2O.

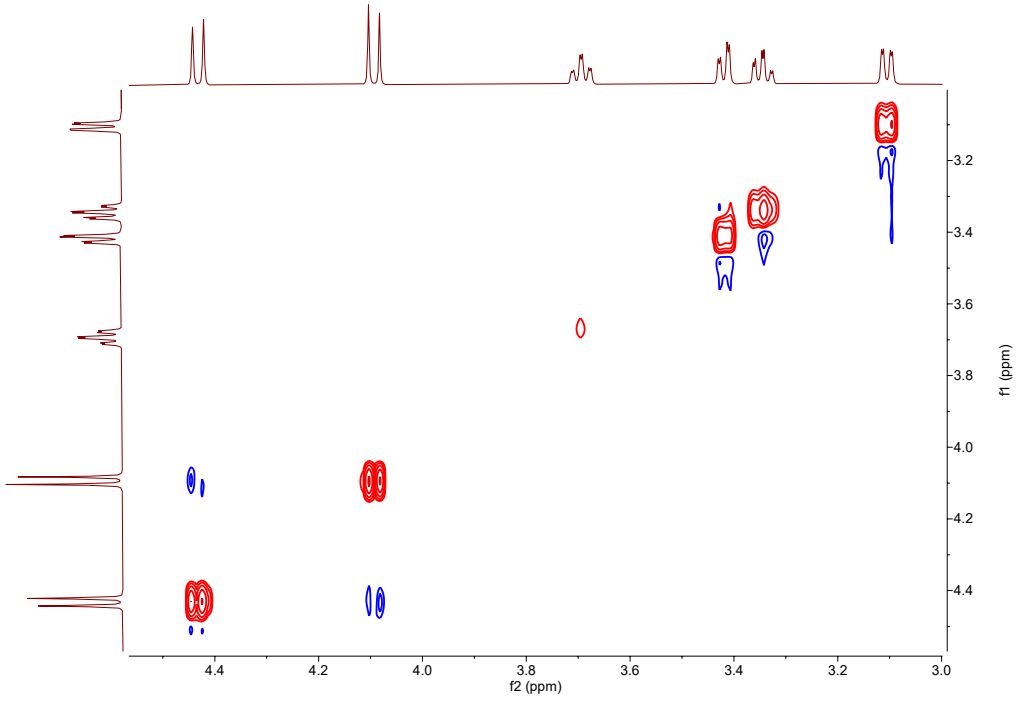

Figure S4. Selected area of the two-dimensional (^{1}H,^{1}H)–NOESY spectra of Ti-DOTA in D_2O.

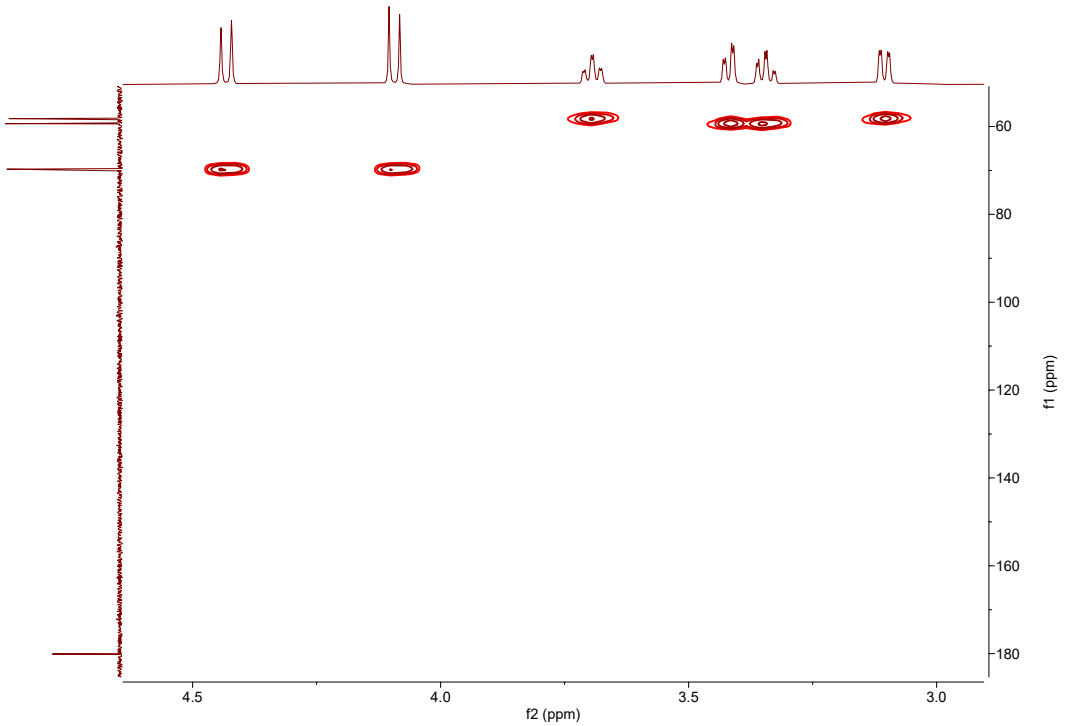

Figure S5. Selected area of the two-dimensional (HSQC) spectra of Ti-DOTA in D_2O.

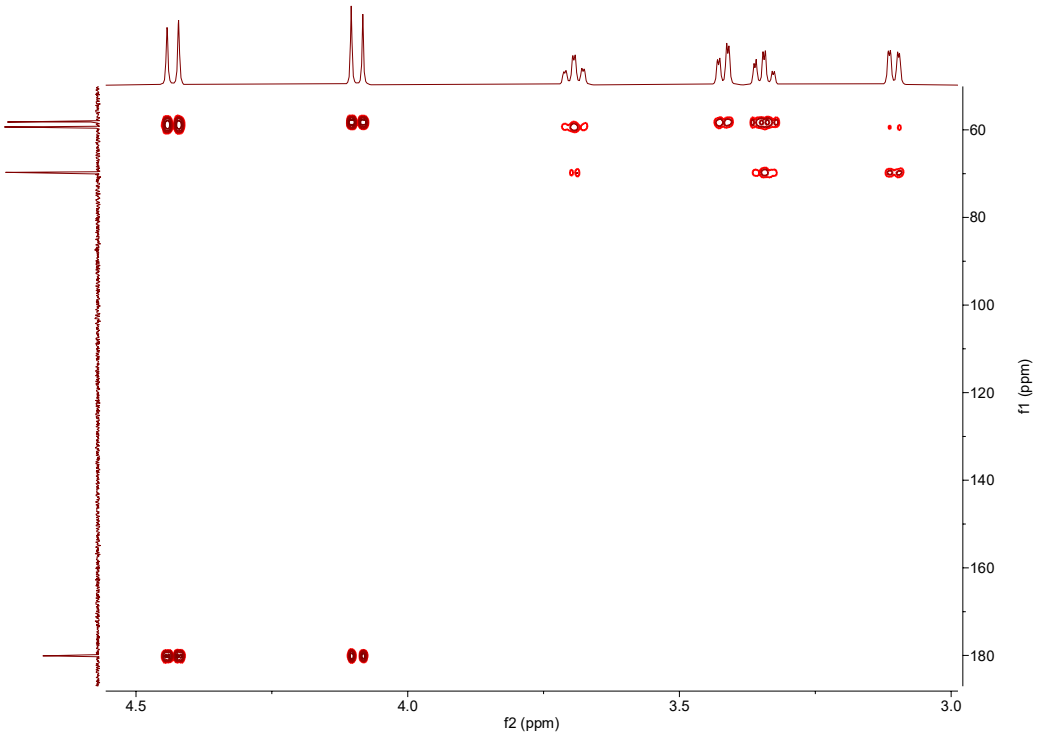

Figure S6. Selected area of the two-dimensional (HMBC) spectra of Ti-DOTA in D_2O.

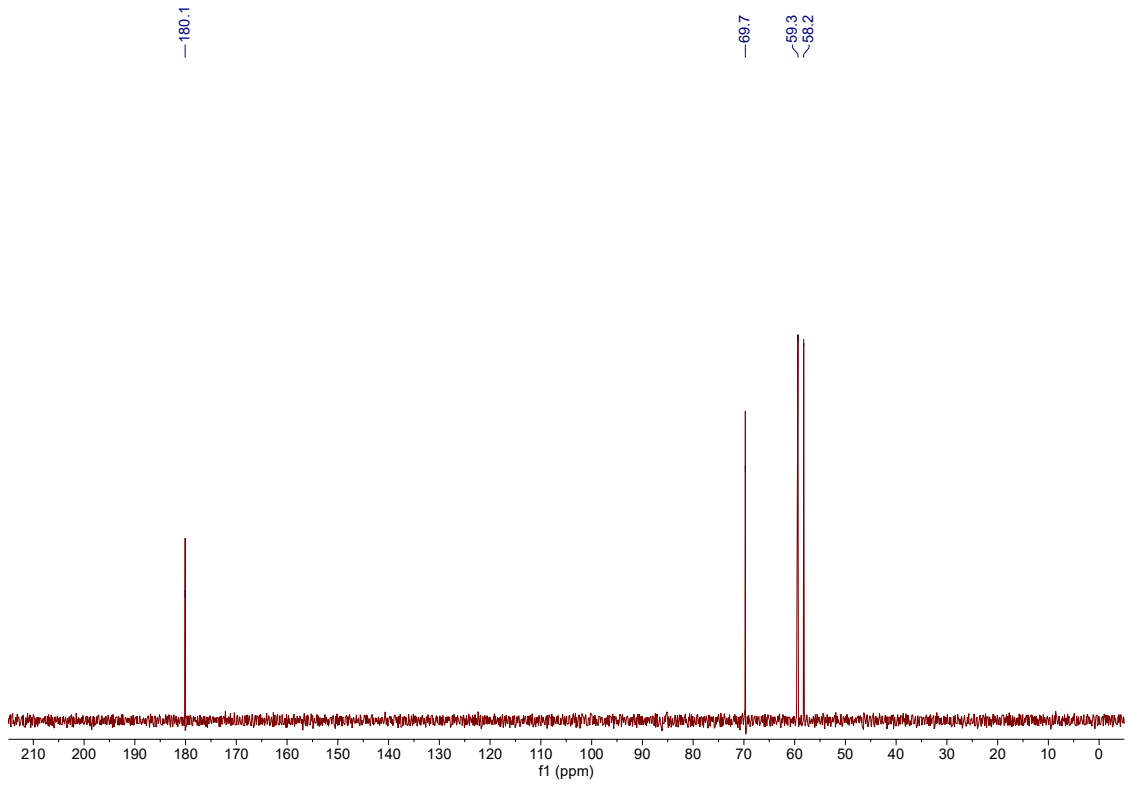

Figure S7. ^{13}C NMR spectrum of Ti-DOTA in D_2O.

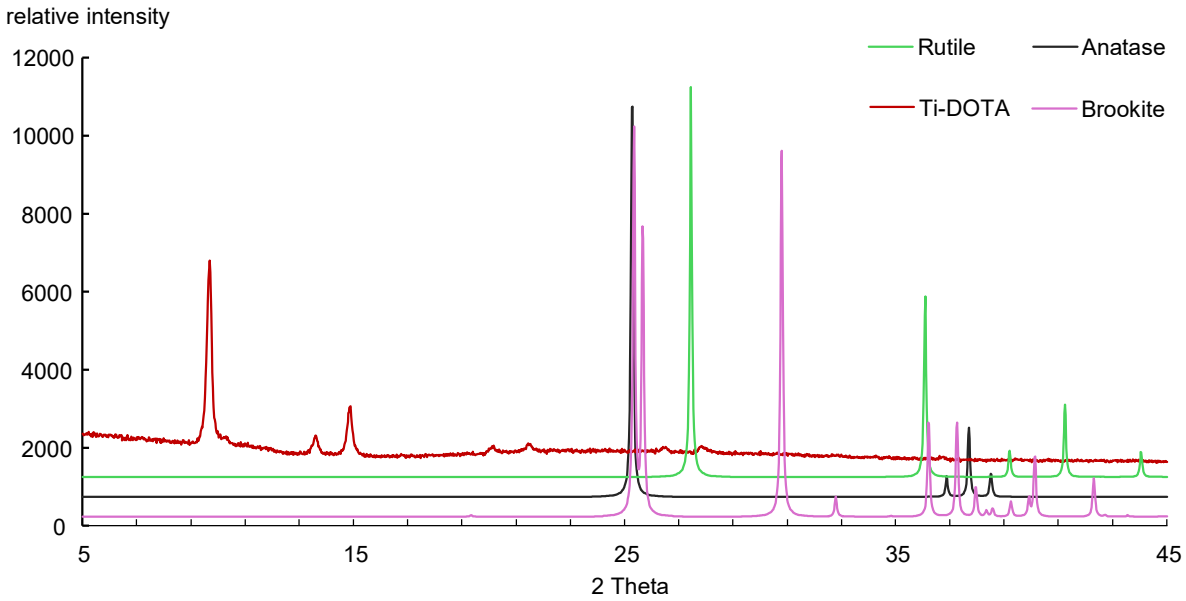

Figure S8. Powder X-ray patterns of Ti-DOTA (after drying in an oven for 12 h, and then further dried under vacuum), and TiO_2 (rutile, COD ID:9004141;[23] and anatase, COD ID:5000223;[24] and brookite, COD ID:9004138[23]). Wavelength: 1.5406 Å (Copper K_α).

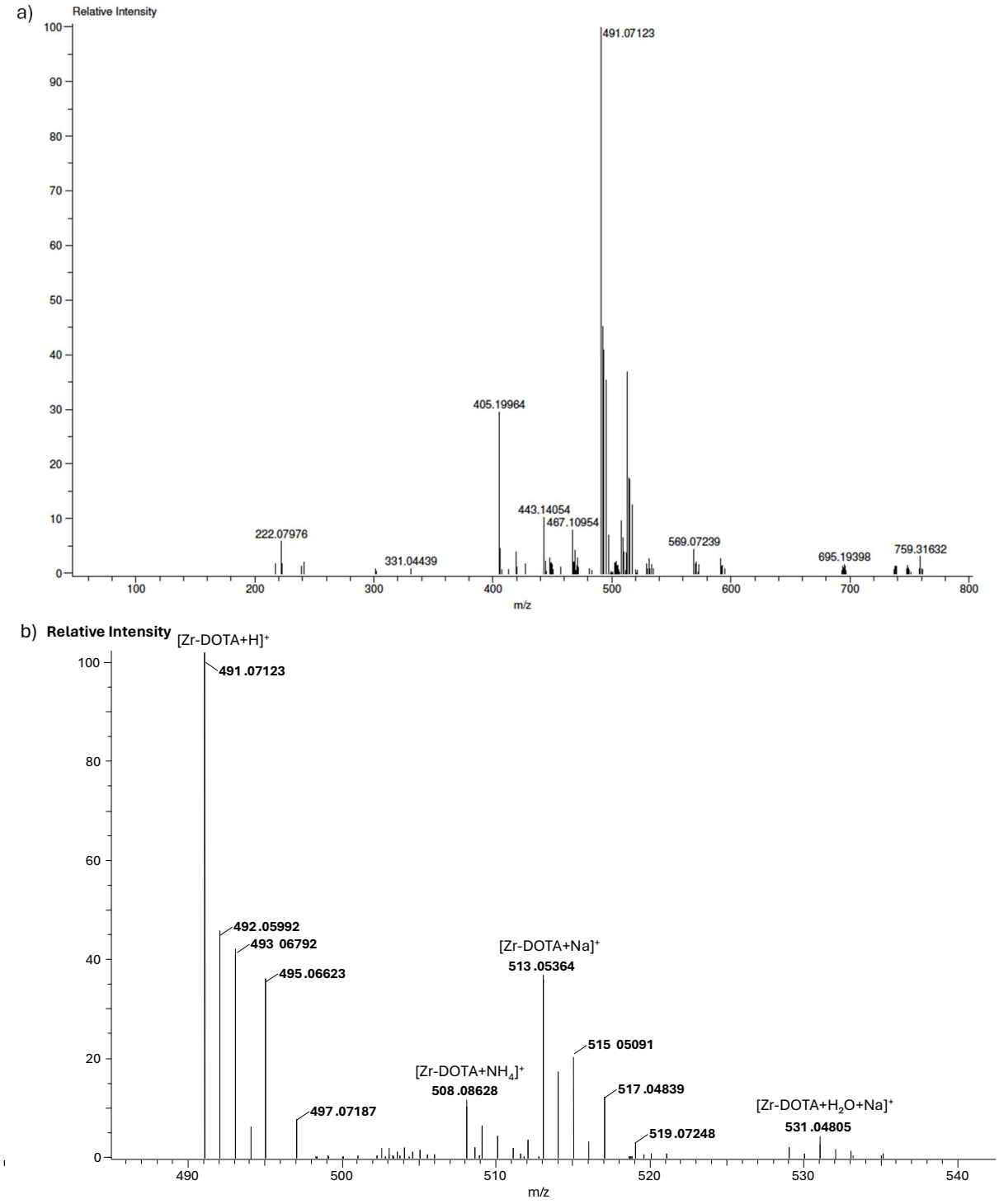

Figure S9. HR-MS (ESI$^+$) spectrum of Zr-DOTA: a) full spectrum, and b) expanded region near the base peak at 491.07123 m/z.

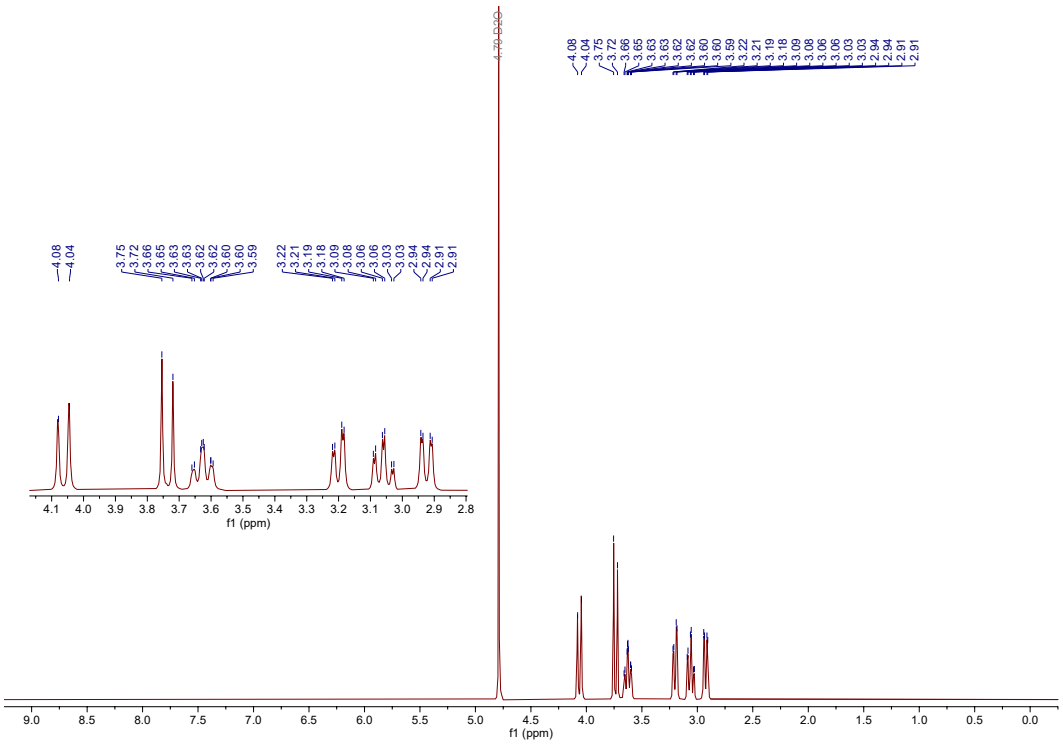

Figure S10. ^{1}H NMR spectrum of Zr-DOTA in D_2O.

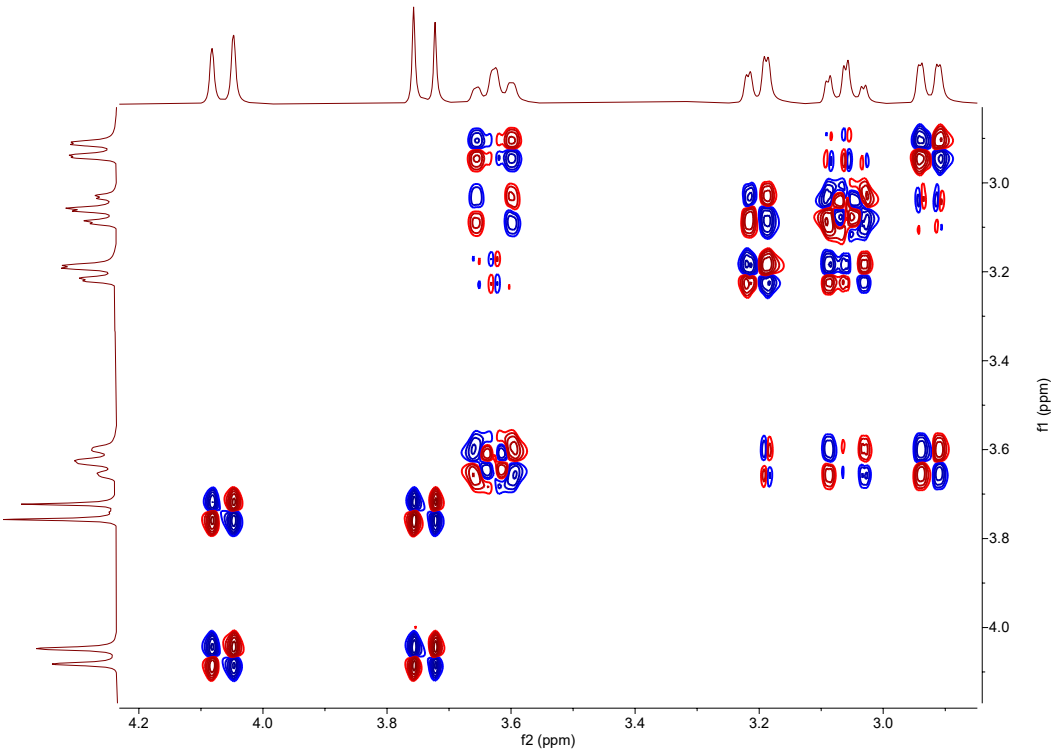

Figure S11. Selected area of the two-dimensional (^{1}H,^{1}H)–COSY spectra of Zr-DOTA in D_2O.

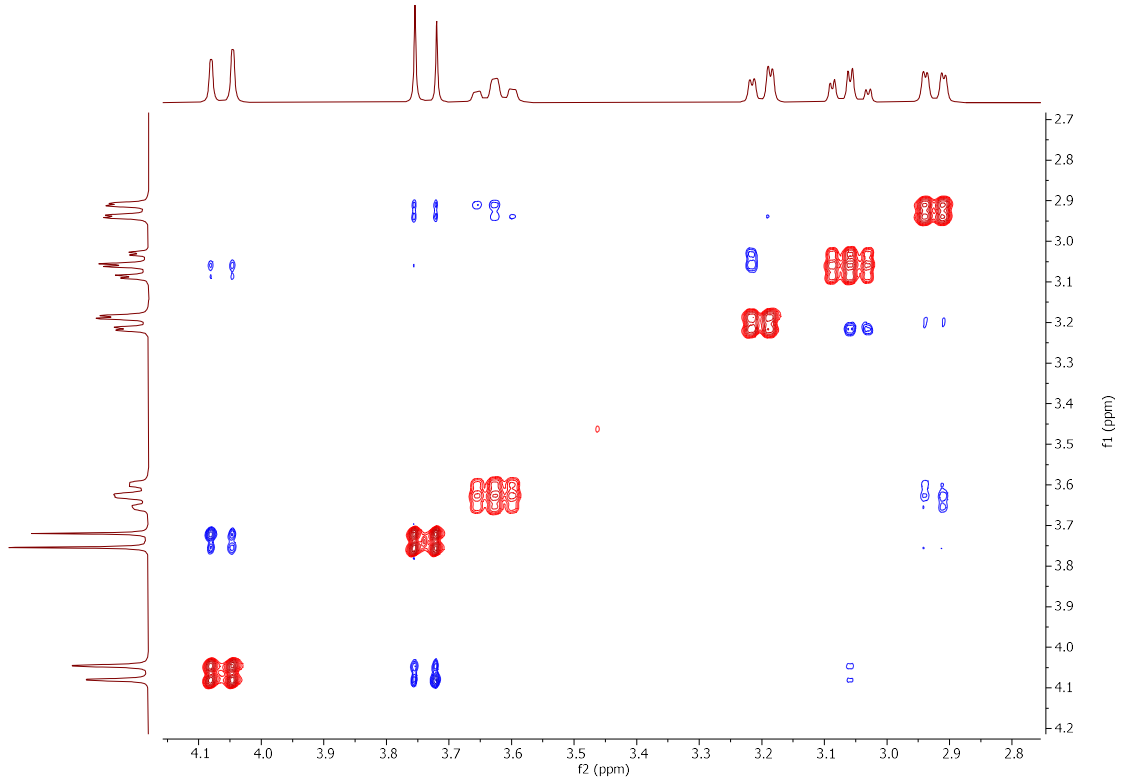

Figure S12. Selected area of the two-dimensional (^{1}H,^{1}H)–NOESY spectra of Zr-DOTA in D_2O.

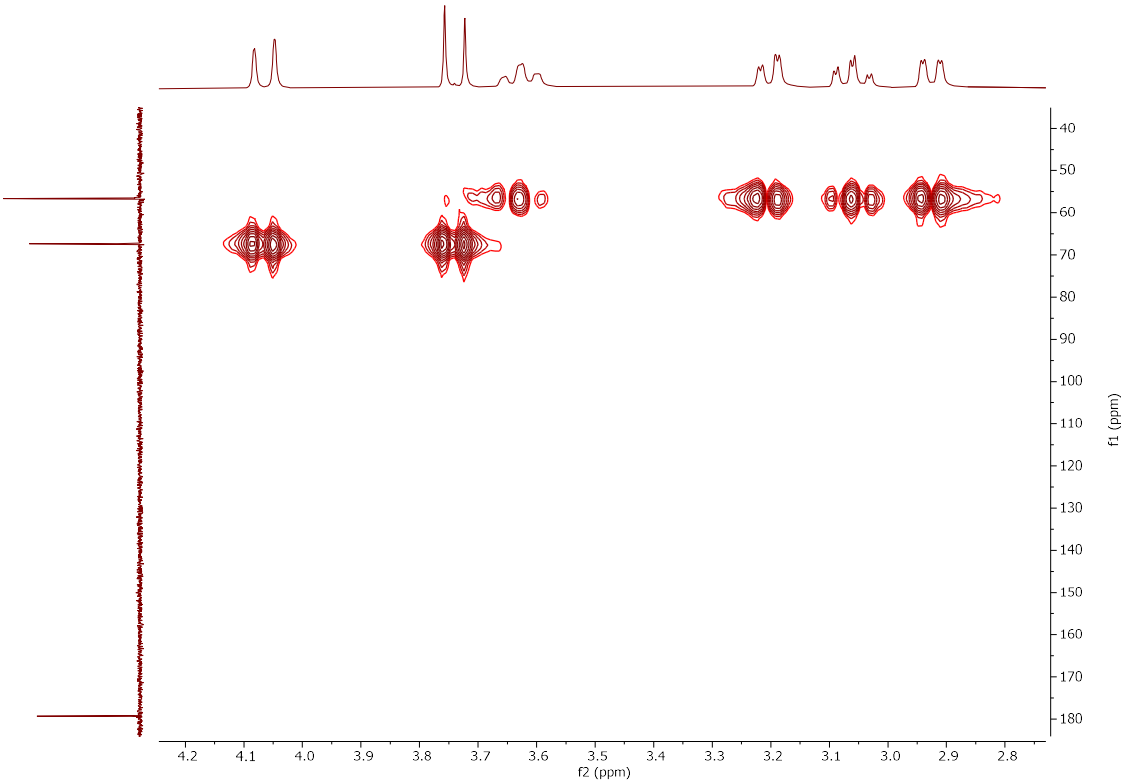

Figure S13. Selected area of the two-dimensional (HMQC) spectra of Zr-DOTA in D_2O.

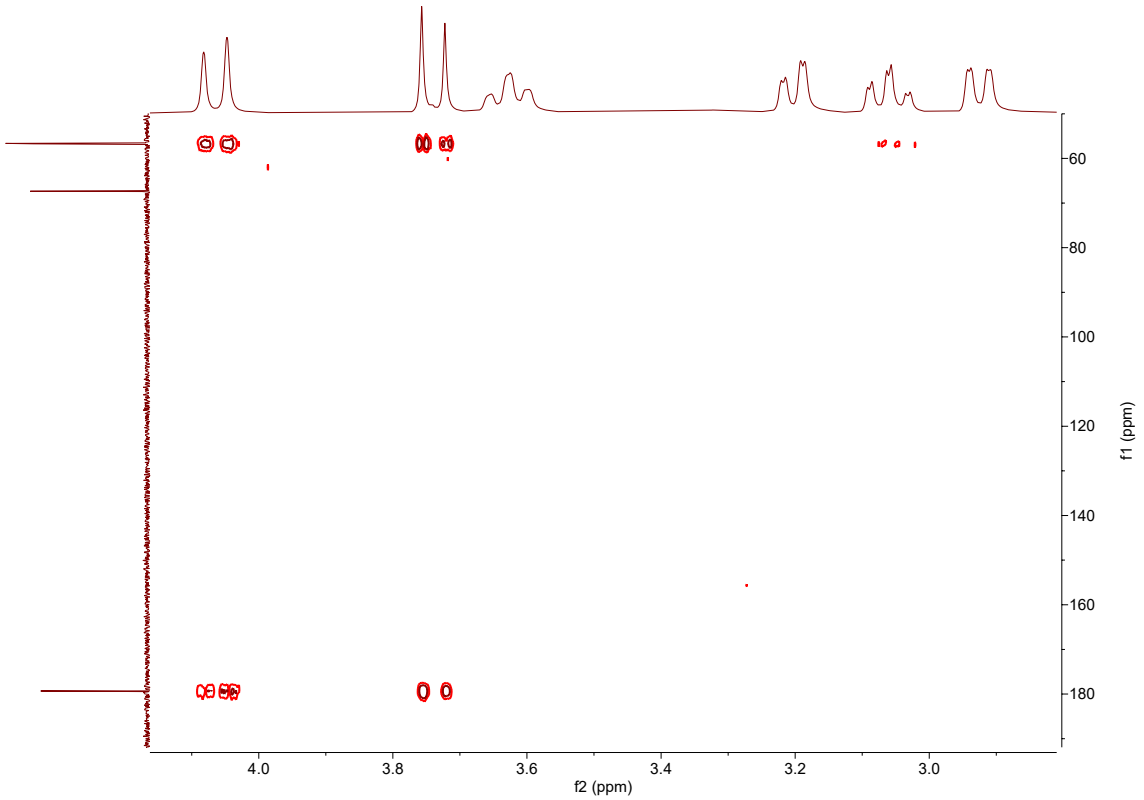

Figure S14. Selected area of the two-dimensional (HMBC) spectra of Zr-DOTA in D_2O.

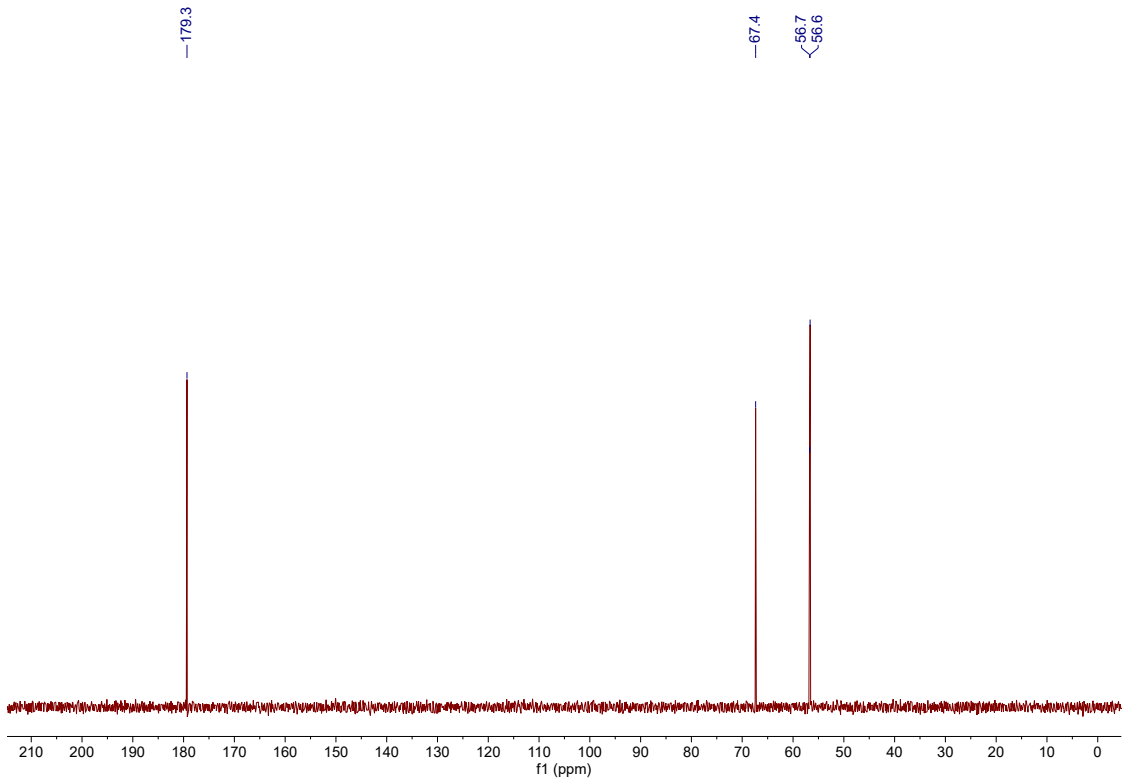

Figure S15. ^{13}C NMR spectrum of Zr-DOTA in D_2O.

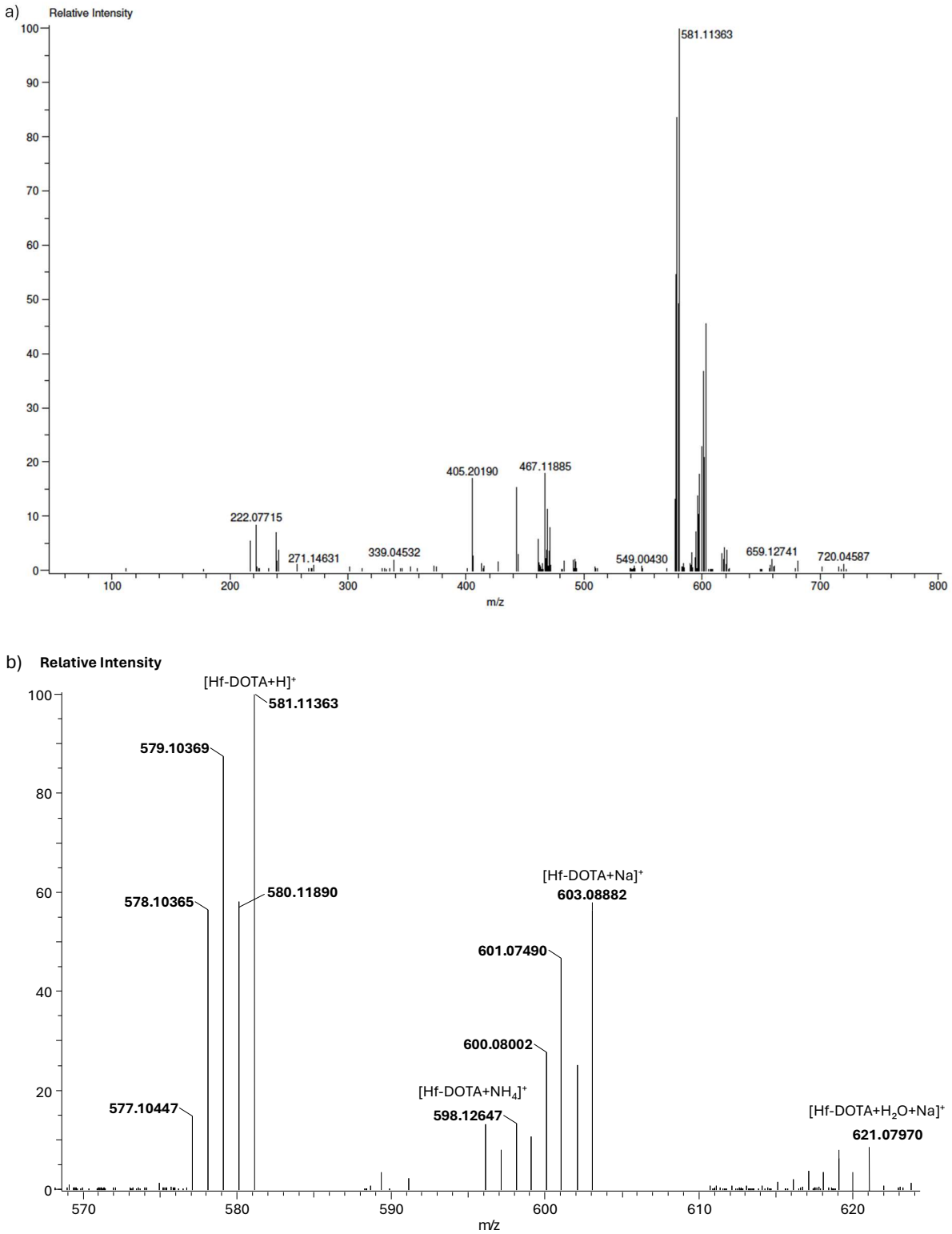

Figure S16. HR-MS (ESI$^+$) spectrum of Hf-DOTA: a) full spectrum, and b) expanded region near the base peak at 581.11363 m/z.

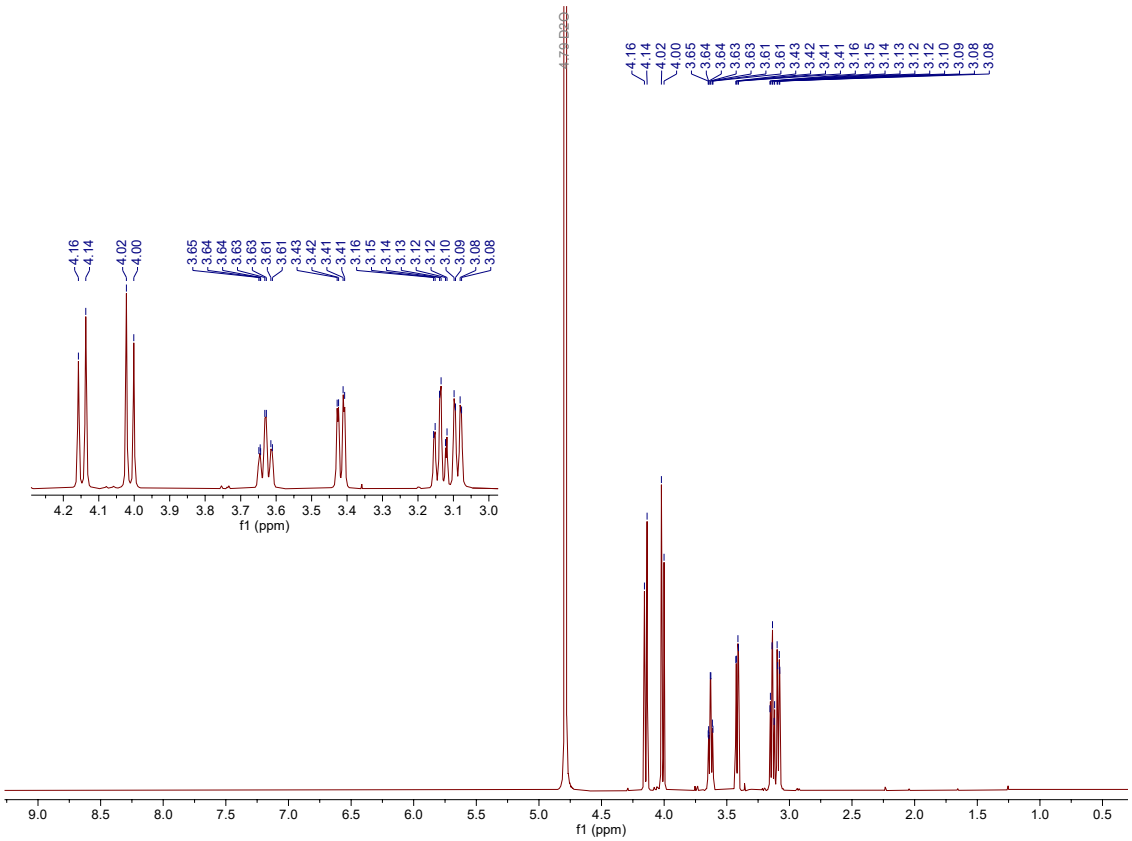

Figure S17. ^{1}H NMR spectrum of Hf-DOTA in D_2O.

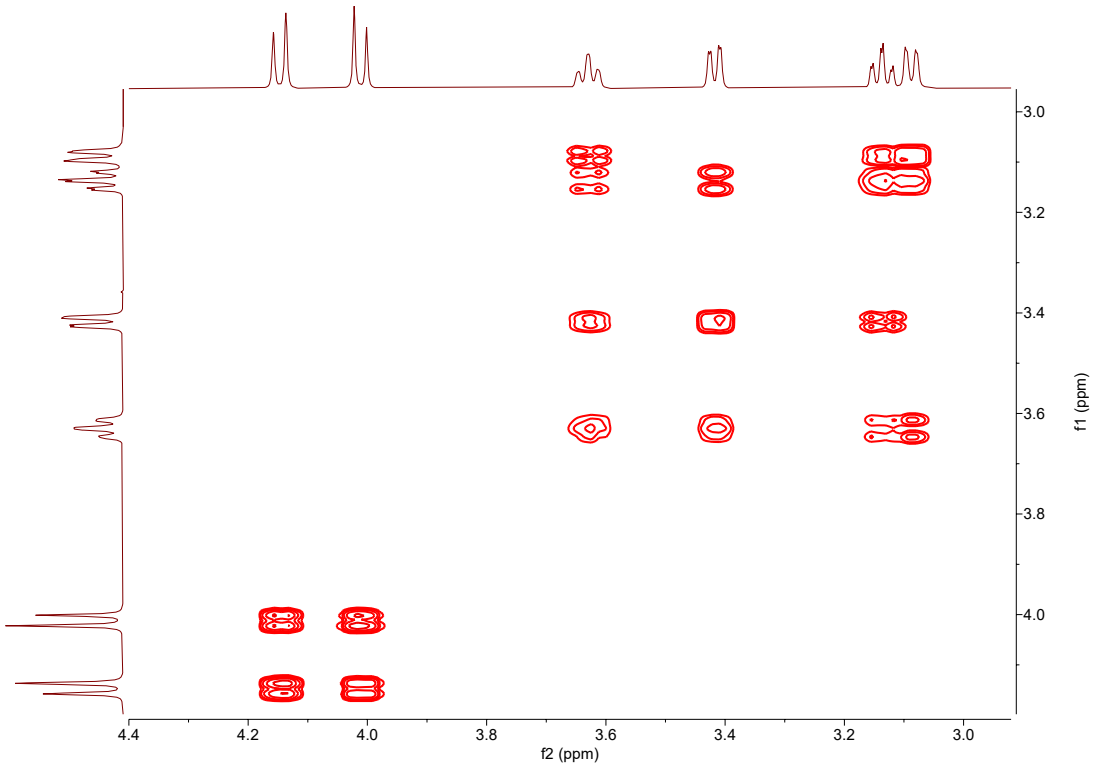

Figure S18. Selected area of the two-dimensional (^{1}H,^{1}H)–COSY spectra of Hf-DOTA in D_2O.

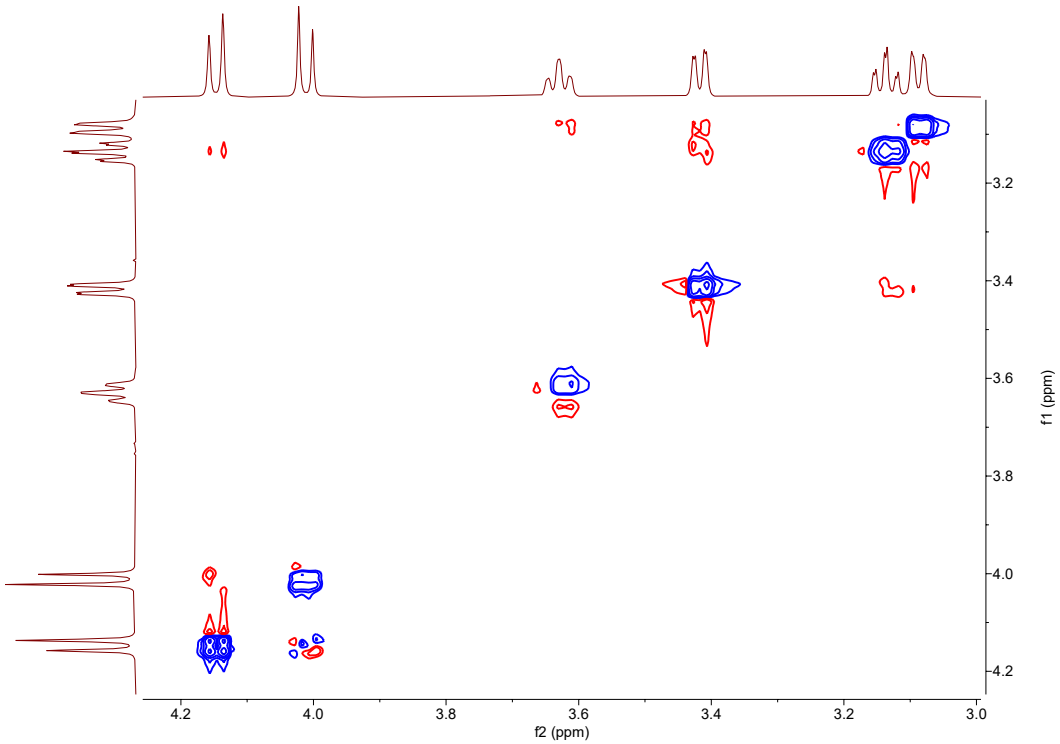

Figure S19. Selected area of the two-dimensional (^{1}H,^{1}H)–NOESY spectra of Hf-DOTA in D_2O.

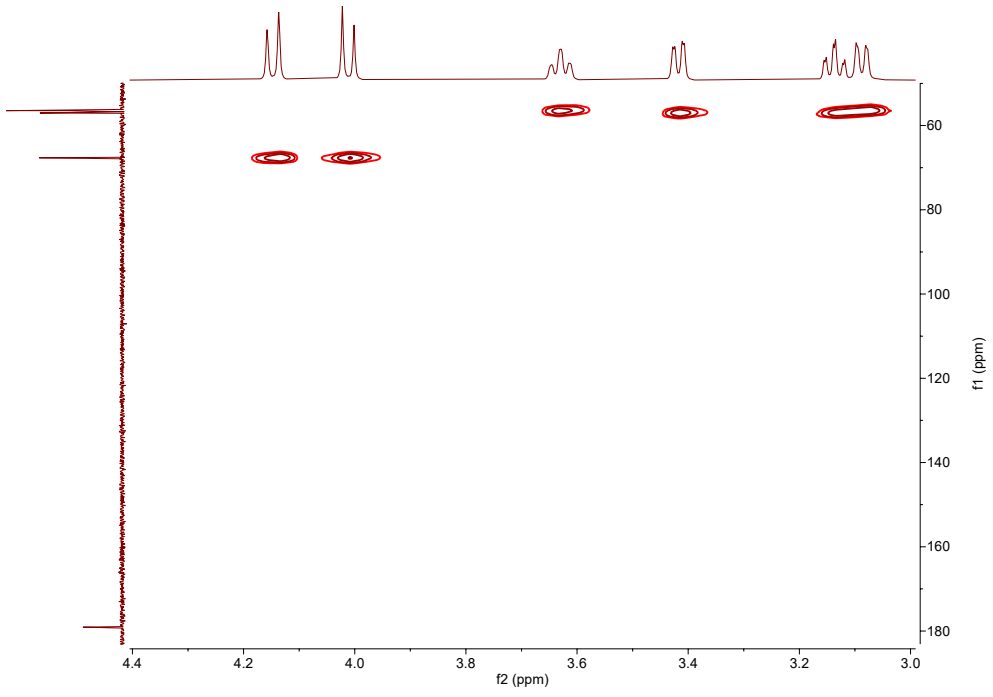

Figure S20. Selected area of the two-dimensional (HSQC) spectra of Hf-DOTA in D_2O.

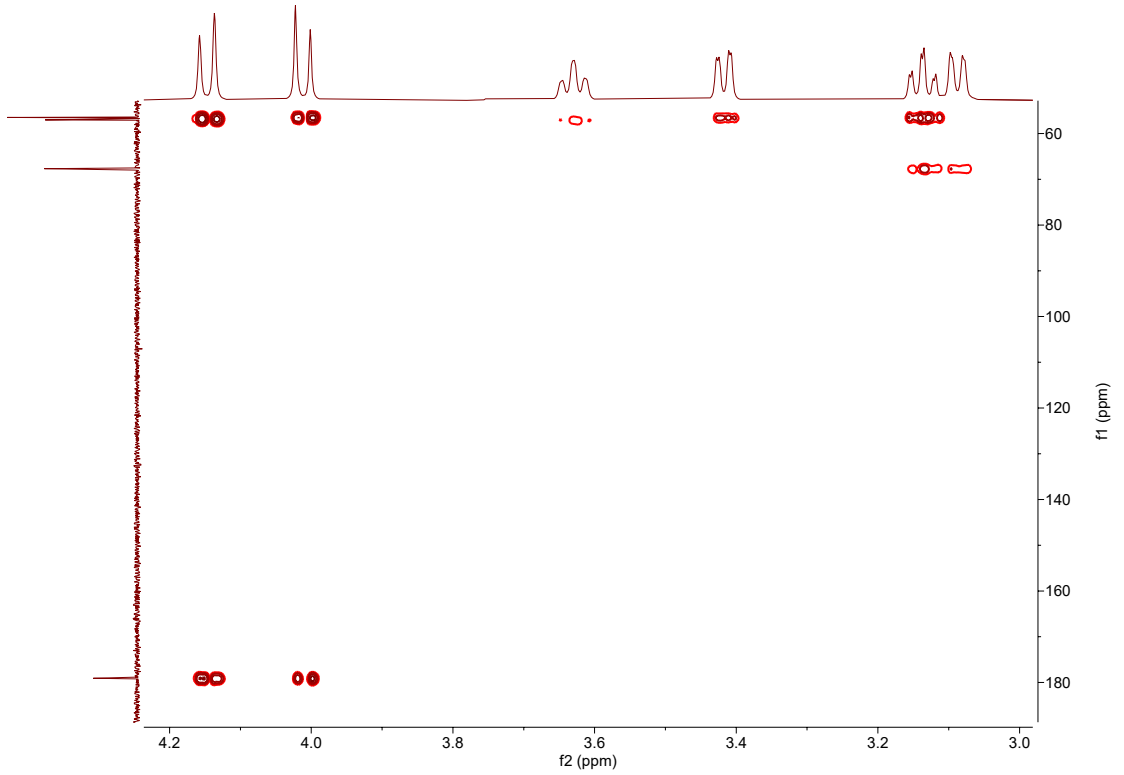

Figure S21. Selected area of the two-dimensional (HMBC) spectra of Hf-DOTA in D_2O.

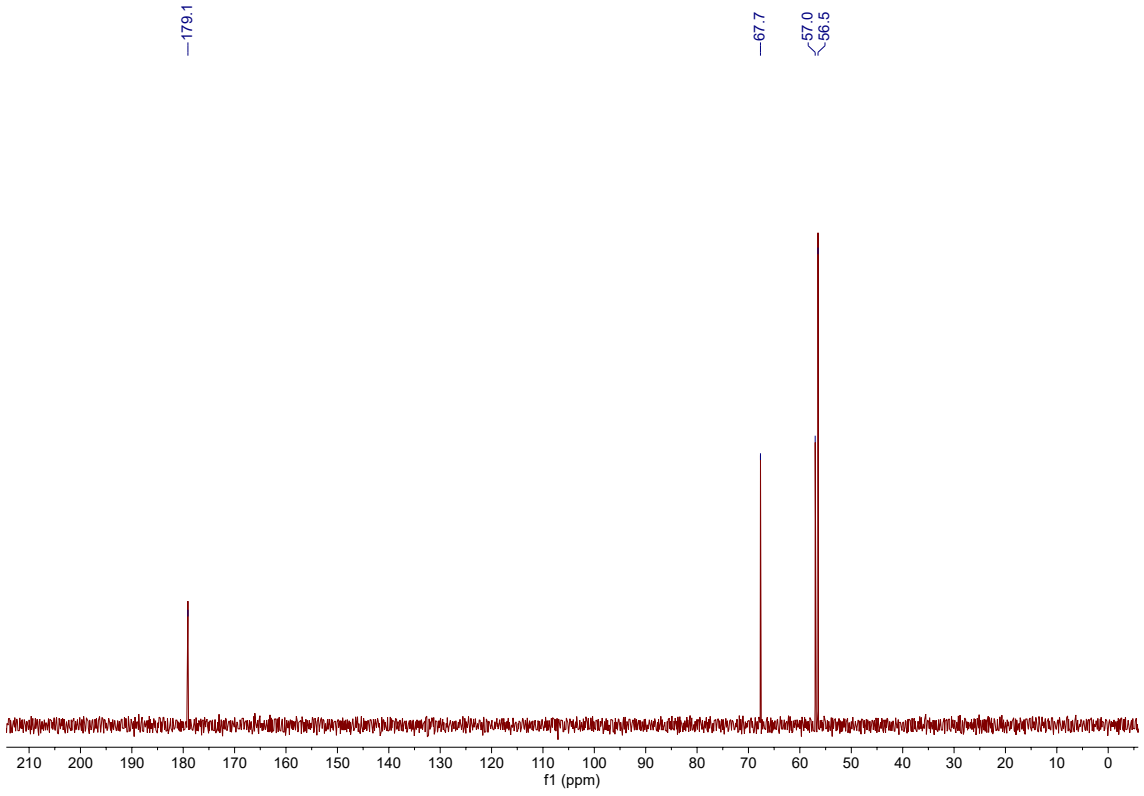

Figure S22. ^{13}C NMR spectrum of Hf-DOTA in D_2O.

Comments on the Crystallographic Experiments on Ti- and Hf-DOTA Structures

Both the Ti-DOTA and Hf-DOTA crystals were grown by dissolving the compounds in boiling water then slowly cooled down to room temperature. Both crystals are notoriously small and brittle thin flakes. Without exception they suffer from rotational twinning around the 4-fold rotation axis (c-axis). Indications of inversion twinning are also present in some case. For both complexes there are two molecules in the asymmetric unit, one more positionally disordered than the other.

The space group used for structure solution and refinement is P_{4mm} (no. 99), albeit a noticeable degree of space group ambiguity exists, likely due to the twinning issues.

The previously published structure of Zr-DOTA[22] also has two complexes in the asymmetric unit, the space group assigned is P_{4cc} (no. 103). That structure does however contain solvent water molecules.

Refinement of Ti-DOTA is very difficult, but the integrity of the (coordinating) atomic species is established, as is the coordination sphere.

Refinement of Hf-DOTA is also difficult, but again the integrity of the (coordinating) atomic species is established, as is the coordination sphere. Also, the two enantiomers can be separated for one of the two complexes in the asymmetric unit, albeit using numerous constraints and restraints.

Although the crystallographic R1-values are less than 10% the wR2 and Goodness-of-fit are much affected by the poor structural models. Therefore, and because of the excessive need of model constraints the determinations do not lend themselves to further publication nor deposition in the Cambridge Structural Database.

Tetragonal unit cell parameters at 100K using μ-source MoK_α radiation are: 12.8044(2), 6.5865(2) for Ti-DOTA and 12.8848(3) 6.5638(2) Å for Hf-DOTA.

Instrumentation used is Rigaku Synergy-S with a Hypix-ARC100 detector. Cryocooler Cryostream model 700 from Oxford Cryosystems Ltd.

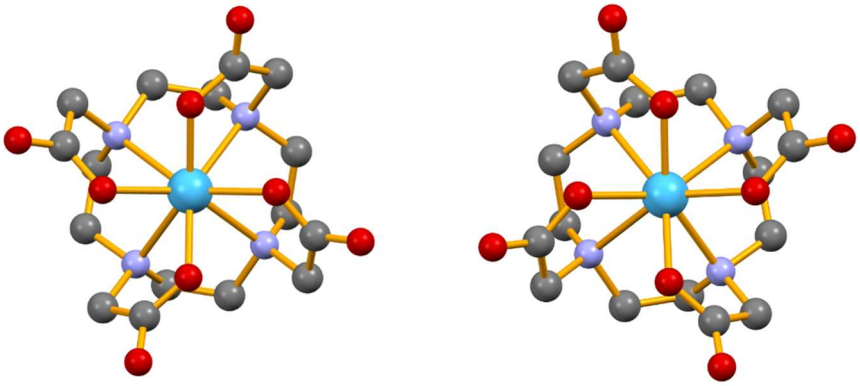

Figure S23. Isotropic atom connectivity for the two enantiomers for the complexes of Hf-DOTA a) $\Delta(\lambda\lambda\lambda\lambda)$ and b) $\Lambda(\delta\delta\delta\delta)$, as deduced from X-ray crystallography, in which the two geometric enantiomers are superimposed. Hydrogen atoms are not shown (blue, Hf; red, O; purple, N and grey, C).

Computational Results on M-DOTA Structures

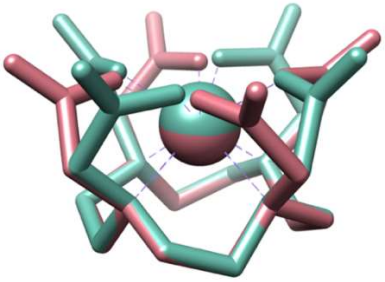

Figure S24. Diastereoisomers $\Lambda(\delta\delta\delta\delta)$ (red) and $\Delta(\delta\delta\delta\delta)$ (green) of Ti-DOTA complex. The frozen geometries were aligned to each other by minimizing the RMSD of the four nitrogen atoms. Hydrogen atoms are omitted for clarity.

In addition to the most commonly observed diastereomers $\Lambda(\delta\delta\delta\delta)$ (SAP, see Figure S23) and $\Delta(\delta\delta\delta\delta)$ (TSAP), another alternative configuration with stereodescriptor $\Delta(\delta\lambda\delta\lambda)$ has been modelled in previous computational studies aiming to estimate the thermodynamic stability of potential Zr-DOTA radiotracers.[25] Such geometry is characterized by a squeezed macrocyclic ring where the distances between each pair of distal N atoms, which are almost identical in the $\Lambda(\delta\delta\delta\delta)$ and $\Delta(\delta\delta\delta\delta)$ geometries, differ by more than 1 Å (orange in Figure S24). While the ligand alone is more stable in the conformation observed in the $\Delta(\delta\lambda\delta\lambda)$ complexes than in $\Lambda(\delta\delta\delta\delta)$ ones (0.8 kcal mol^{-1} for Zr-DOTA, see models ID M24 and M25 Table S2), all its complexes were found to be less stable in the $\Delta(\delta\lambda\delta\lambda)$ than in the $\Lambda(\delta\delta\delta\delta)$ configuration by 7-9 kcal mol^{-1} (Table S2). Clearly, the metal-coordinating environment offered by the ligand conformation on the $\Lambda(\delta\delta\delta\delta)$ geometry is the most suitable for these M^{4+} ions, and the overall stabilization resulting from the ligand–metal interaction greatly overcomes the small additional strain in the organic part of the ligand such conformation.

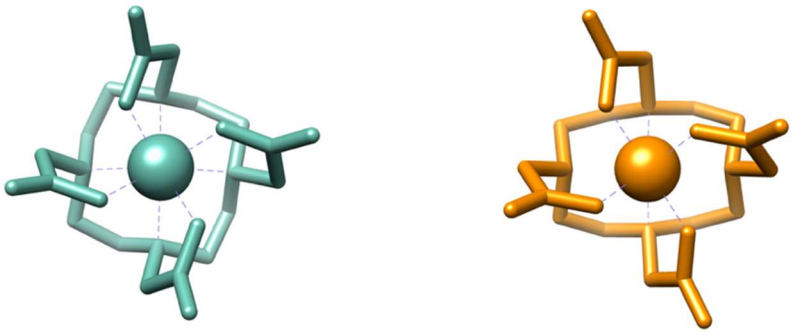

Figure S25. DFT-optimized geometries of Ti-DOTA with $\Delta(\delta\delta\delta\delta)$ (green) and $\Delta(\delta\lambda\delta\lambda)$ (orange). Hydrogen atoms are omitted for clarity.

Table S2. Energy components computed for all species modelled in this work. See Computational Details section for a definition of each component.

ID	Description	$E_{\square}^{TZ}$ [a.u.]	G_{qh}^{298K} [a.u.]	$E_{\square}^{QZ}$ [a.u.]	$G_{\square}^{298K\ [1M]}$ [a.u.]	ΔG[a] [kcalmol^{-1}]
M1	$DOTA^{4-}$	-1444.560977	0.349696	-1444.652889	-1444.300174	0.0 (M1)
M2	$DOTA^{4-}$	-1444.532842	0.348981	-1444.624561	-1444.272562	17.3 (M1)
M3	$EDTA^{4-}$	-1099.513977	0.176944	-1099.580275	-1099.400312	0.0 (M3)
M4	$EDTA^{4-}$	-1099.511351	0.176965	-1099.577559	-1099.397575	1.7 (M3)
M5	$(H_2O)_{19}$	-1451.653644	0.385587	-1451.775432	-1451.386827	-
M6	$[Ti(H_2O)_{19}]^{4+}$	-2300.501262	0.388848	-2300.642688	-2300.250821	-
M7	$[Zr(H_2O)_{19}]^{4+}$	-1498.300648	0.397043	-1498.431833	-1498.031772	-
M8	$[Hf(H_2O)_{19}]^{4+}$	-1499.991233	0.395145	-1500.118394	-1499.720230	-
M9	Ti-DOTA $\Lambda(\delta\delta\delta\delta)$	-2293.577352	0.368658	-2293.686578	-2293.314901	0.0 (M9)
M10	Ti-DOTA $\Delta(\delta\delta\delta\delta)$	-2293.568427	0.368518	-2293.677645	-2293.306109	5.5 (M9)
M11	Ti-DOTA $\Delta(\delta\lambda\delta\lambda)$	-2293.562784	0.368602	-2293.672087	-2293.300467	9.1 (M9)
M12	Zr-DOTA $\Lambda(\delta\delta\delta\delta)$	-1491.325635	0.365524	-1491.425558	-1491.057015	0.0 (M12)
M13	Zr-DOTA $\Delta(\delta\delta\delta\delta)$	-1491.320051	0.366149	-1491.419803	-1491.050635	4.0 (M12)
M14	Zr-DOTA $\Delta(\delta\lambda\delta\lambda)$	-1491.316256	0.366913	-1491.416142	-1491.046211	6.8 (M12)
M15	Hf-DOTA $\Lambda(\delta\delta\delta\delta)$	-1493.033345	0.365764	-1493.127979	-1492.759197	0.0 (M13)
M16	Hf-DOTA $\Delta(\delta\delta\delta\delta)$	-1493.026092	0.365861	-1493.120774	-1492.751894	4.6 (M13)
M17	Hf-DOTA $\Delta(\delta\lambda\delta\lambda)$	-1493.023522	0.367243	-1493.118263	-1492.748001	7.0 (M13)
M18	Ti-EDTA $\Lambda(\delta)$	-1948.503130	0.188516	-1948.587953	-1948.396418	0.0 (M18)
M19	Ti-EDTA $\Delta(\delta)$	-1948.491417	0.190624	-1948.576303	-1948.382660	8.6 (M18)
M20	Zr-EDTA $\Lambda(\delta)$	-1146.268536	0.190168	-1146.342965	-1146.149778	0.0 (M20)
M21	Zr-EDTA $\Delta(\delta)$	-1146.262172	0.189022	-1146.336562	-1146.144522	3.3 (M20)
M22	Hf-EDTA $\Lambda(\delta)$	-1147.970643	0.187708	-1148.040643	-1147.849917	0.0 (M22)
M23	Hf-EDTA $\Delta(\delta)$	-1147.964902	0.189449	-1148.034819	-1147.842352	4.7 (M22)
M24	DOTA-4 (geom. from Zr-DOTA $\Lambda(\delta\delta\delta\delta)$ M12)	-	-	-1444.553388	-1444.550369	0.0 (M24)[b]
M25	DOTA-4 (geom. from Zr-DOTA $\Delta(\delta\lambda\delta\lambda)$ M14)	-	-	-1444.554630	-1444.551611	-0.8 (M24)[b]

[a] Calculated relative to the reference system specified in parenthesis. [b] Value corresponding to $\Delta E_{\square}^{QZ}$, *i.e.*, no thermal correction included.

Table S3. Geometric parameters for non-capped M-DOTA complexes.

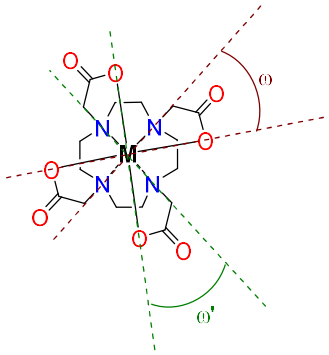

$\tau_8 = (\pi/2-(\omega+\omega'))/\theta$
$\theta = \cos^{-1}(1/\sqrt{2})$

M-DOTA	IR[a] (Å)	d_{M-N4}[a] (Å)	d_{M-O4}[a] (Å)	ω (°)	ω' (°)	τ_8[b]	Geometry	Isomer	Refs
Bi(III)	1.17	1.434	1.112	25.46	26.36	0.84	TSAP	$\Delta(\delta\delta\delta\delta)$	26
Bi(III)	1.17	1.450	1.116	26.18	26.18	0.83	TSAP	$\Delta(\delta\delta\delta\delta)$	27
Tl(III)	0.98	1.322	1.254	24.92	25.99	0.86	TSAP	$\Delta(\delta\delta\delta\delta)$	28
Lu(III)	0.97	1.445	1.077	25.24	25.31	0.87	TSAP	$\Delta(\delta\delta\delta\delta)$	29
Sc(III)	0.87	1.300	1.037	27.92	27.92	0.76	TSAP	$\Lambda(\lambda\lambda\lambda\lambda)$	30
Zr(IV)	0.84	1.356	1.004	41.50	41.50	0.15	SAP	$\Delta(\lambda\lambda\lambda\lambda)$	22
Zr(IV)	0.84	1.279	1.107	41.75	41.75	0.14	SAP	$\Lambda(\delta\delta\delta\delta)$	22
Zr(IV)[c]	0.84	1.382	0.915	40.55	41.67	0.17	SAP	$\Lambda(\delta\delta\delta\delta)$	this work
Hf(IV)[c]	0.83	1.351	0.937	41.24	41.60	0.16	SAP	$\Lambda(\delta\delta\delta\delta)$	this work
Ti(IV)[c]	0.74	1.278	0.977	43.20	43.43	0.07	SAP	$\Lambda(\delta\delta\delta\delta)$	this work

[a] IR = ionic radius for 8-coordinate complexes, see ref. 31, and d_{M-N4} and d_{M-O4} = metal departure from the least square mean planes of N_4 and O_4. [b] Index parameter: $\tau_8 = (\pi/2-(\omega+\omega'))/\theta$, with $\theta = \cos^{-1}(1/\sqrt{2})$, where ω and ω ' are the two twisted valence angles between bidentate ligands (here O-N for DOTA). When τ_8 is close to 0 the geometry is similar to square-antiprism (SAP), while if τ_8 is close to 1 the geometry is similar to twisted square-antiprism (TSAP). [c] Based on optimized geometry determined by DFT (see DFT discussions).

Stability Studies of Ti-DOTA Complex

Preparation of phosphate-buffered Saline (100 mM). NaH_2PO_4 (2.939 g, 24.5 mmol) was introduced into a beaker (1L) and dissolved in Milli-Q water (500 mL) by using a gentle stirring, then the resulting solution was transferred to a volumetric flask (1 L). $Na_2H_2PO_4$ (10.704 g, 75.4 mmol) was dissolved in Milli-Q water (500 mL) and around 400-450 mL of the resulting solution was transferred to the same volumetric flask as the earlier prepared NaH_2PO_4 solution. Then, pH value of the resulting solution in the volumetric flask was measured constantly by pH-meter while the remaining 50-100 mL of $Na_2H_2PO_4$ solution were added dropwise until the desired pH value of 7.4 was reached for the phosphate-buffered saline solution.

Preparation of solutions of metal cations and Ti-DOTA complex in PBS. $MgSO_4$ (0.012 g, 0.1 mmol), $FeCl_3.6H_2O$ (0.027 g, 0.1 mmol), $CoCl_2$ (0.013 g, 0.1 mmol), $CuSO_4.5H_2O$ (0.025 g, 0.1 mmol), $ZnCl_2$ (0.014 g, 0.1 mmol), and Ti-DOTA (0.005 g, 0.01mmol) were all introduced into vials and dissolved in PBS (10 mL) by using stirring and heating.

Performing of stability studies of Ti-DOTA complex. To the solutions of metal cations [iron(III) chloride hexahydrate, zinc(II) chloride, cobalt(II) chloride, copper(II) sulfate pentahydrate, magnesium(II) sulfate] (10 mM, 1 mL), was added Ti-DOTA complex (1 mM, 1 mL) in PBS, pH 7.4. The resulting solutions were incubated at 37 ºC for 160 hours in an oil bath. Then, the

dissociation of titanium from Ti-DOTA complex was monitored by HPLC analysis at 3, 44 and 92 h time points.

Table S4. Stability of Ti-DOTA complex with various metal cations (PBS, pH 7.4) and EDTA at 37 °C.

Entry	Ligand	Metal cation	Time (h)	Intact Ti-DOTA (%)[a]
1	-	-	92	99
2	-	Mg^{2+}	3	99
			44	99
			92	99
3	-	Fe^{3+}	3	99
			44	98
			92	98
4	-	Co^{2+}	3	99
			44	99
			92	98
5	-	Cu^{2+}	3	99
			44	99
			92	91
6	-	Zn^{2+}	3	99
			44	98
			92	95
7	EDTA	-	92	97

[a] Calculated using HPLC analysis.

Thermodynamic Studies by DFT for M-DOTA Complexes

Table S5. Gibbs free energy of complexation calculated with the PBE-GD3MBJ-SMD(water) model considering the formation of M-DOTA complexes starting from the corresponding tetra-cationic metal atom and tetra-anionic DOTA ligand in water (implicit solvent model).

$$[M(H_2O)_{19}]^{+4} + DOTA^{-4} \xrightleftharpoons{\Delta G_{complexation}} M(DOTA) + (H_2O)_{19}$$

$$M(EDTA) + DOTA^{-4} \xrightleftharpoons{\Delta G_{ligand\_exchange}} M(DOTA) + EDTA^{-4}$$

Species	$\Delta G_{complexation}$ (kcal mol^{-1})	$\Delta G_{ligand\_exchange}$ (kcal mol^{-1})
Ti-DOTA $\Lambda(\delta\delta\delta\delta)$	-94.6	-11.7
Zr-DOTA $\Lambda(\delta\delta\delta\delta)$	-70.2	-4.6
Hf-DOTA $\Lambda(\delta\delta\delta\delta)$	-78.8	-5.9

^{45}Ti: Separation methods and synthesis of [^{45}Ti]Ti-DOTA complex

Radionuclidic purity (RNP) Compares the activity of a specific radionuclide to the total activity.	$$RNP = \frac{Activity\ of\ {}^{45}Ti}{Total\ activity} \times 100\ \%$$
Extraction efficiency (EE) Compares the extracted amount of a substance to the total amount of that substance used in the extraction. Describes the efficiency of the extraction process.	$$EE = \frac{Activity\ of\ {}^{45}Ti}{Activity\ of\ {}^{45}Ti\ used\ for\ extraction} \times 100\ \%$$
Radiochemical conversion (RCC) Compares the activity of a radiochemical product to the activity of the radionuclide used at the start of the reaction. RCC can be obtained through radio-HPLC. Describes the radiolabeling degree.	$$RCC = \frac{Activity\ of\ {}^{45}Ti\ in\ the\ product}{Activity\ of\ {}^{45}Ti\ at\ the\ start\ of\ reaction} \times 100\ \%$$
Isolation efficiency (IE) Compares the activity of an isolated product to the activity of the crude product used for purification. Describes the efficiency of the isolation process.	$$IE = \frac{Activity\ of\ {}^{45}Ti\ in\ the\ isolated\ product}{Activity\ of\ {}^{45}Ti\ in\ the\ crude\ product} \times 100\ \%$$
Radiochemical yield (RCY) Compares the activity of an isolated radiochemical product to the activity used in the beginning of the process[a] (*i.e.* before separation). Describes the efficiency of the whole process.	$$RCY = \frac{Activity\ of\ {}^{45}Ti\ in\ the\ isolated\ product}{Activity\ of\ {}^{45}Ti\ at\ the\ start\ of\ process} \times 100\ \%$$
Partition Coefficient (K_D) Compares the distribution of a substance in the organic vs. aqueous phase.	$$K_D = \frac{Activity\ of\ {}^{45}Ti\ in\ the\ organic\ phase}{Activity\ of\ {}^{45}Ti\ in\ the\ aqeous\ phase}$$

[a] Before separation of ^{45}Ti from the scandium matrix.

Table S6. Overview of irradiation parameters and activities.

Entry	$Sc(NO_3)_3$ (M)	HNO_3 (M)	Time (min)	Current (µA)	Activity[a] (MBq)	RNP[a] (%)	Activity[b] (MBq)	Cooling time (h)
1	2	0.3	90	10	1126	99.6	855	0.83
2	0.5	0.15	120	25	1008	99.5	365[c]	1.83
3	1.5	0.3	100	15	880	99.4	567	1.5
4	1.5	0.25	120	25	614	97.4	345	1.33
5	1.5	0.3	100	15	1250	99.4	881	1.17
6	1.5	0.05	120	25	311	95.3	225	1.5
7	1.5	0.05	120	25	429	96.6	369	0.66
8	2	0.1	180	20	898	97.0	715	1

[a] Measured at EOB, RNP = radionuclidic purity. [b] Activity used prior extraction. [c] Aliquot (60%) of activity used.

Solid Phase Extraction (SPE)

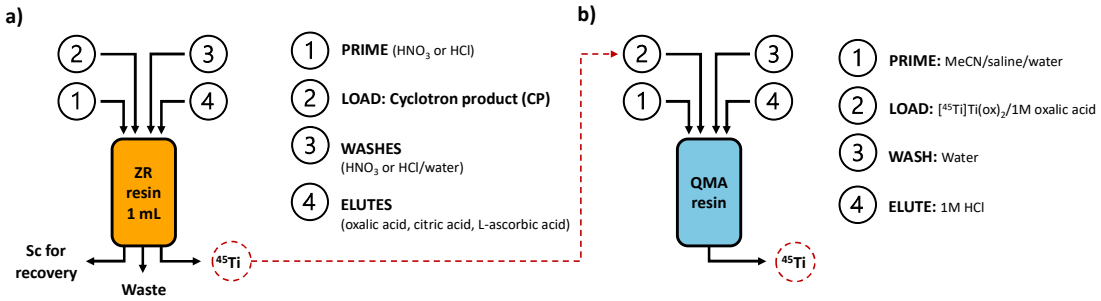

Scheme S1. Representation of the solid-phase extraction (SPE) protocols using the ZR-resin (a) and ZR-resin/QMA-resin (b).

Liquid-Liquid Extraction (LLE)

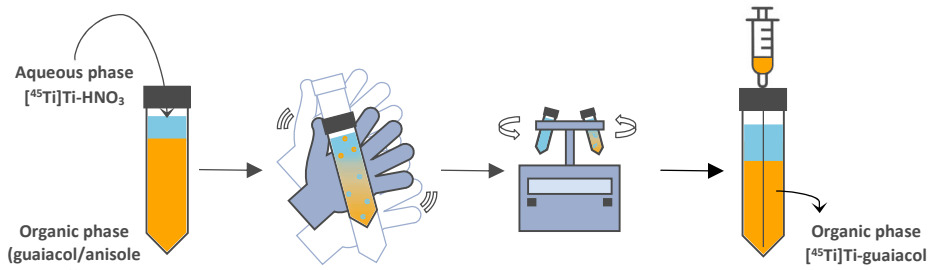

Scheme S2. Representation of the liquid-liquid extraction (LLE) protocol.

The cyclotron product (1.6 mL) was added to a mixture of guaiacol and anisole (9/1; *v/v*; 2.1 mL) in an aqueous/organic ratio of 1/1.3 in a 15 mL centrifuge tube. The centrifuge tube was shaken for 2 min, and then layers were separated using a centrifuge (4000 rpm, 15 min, 20 ^{o}C). An extraction efficiency of 81% (K_D = 11.26) was achieved in this technique. The organic phase (1.75 mL) was isolated and incubated with a DOTA-solution (0.05 M DOTA in 2.5 mL DMSO) in presence of excess pyridine (50 µL) for 15 minutes at 60 ^{o}C. Almost a complete conversion to the desired product ($[^{45}Ti]Ti$-DOTA) was obtained (RCC = 98.2%). The crude product was purified using a preparative HPLC (VP 250/10 Synthra Reeperbahn, 5 µm, 60/40 water/acetonitrile, flowrate 4 mL/min) to obtain 14.9% RCY (d.c., IE = 19%) of the pure product.

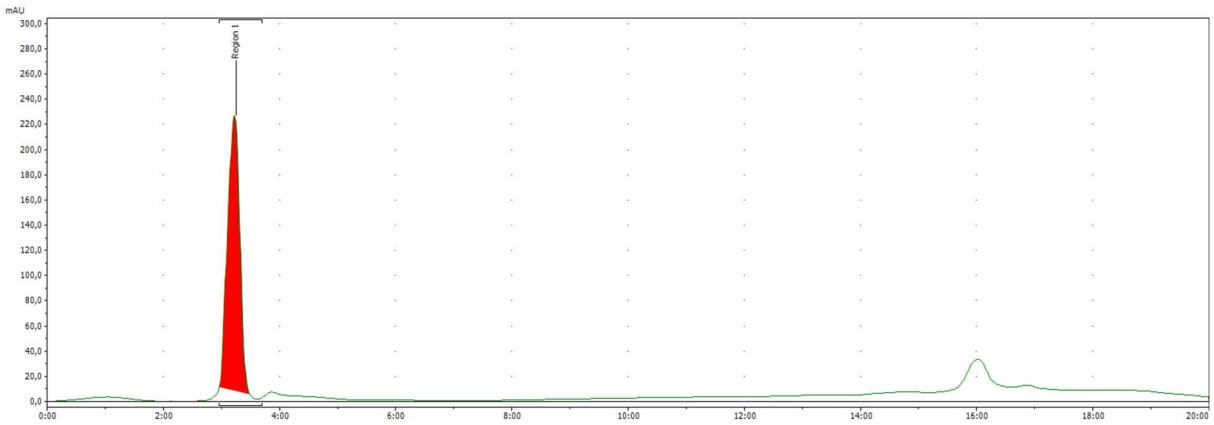

Figure S26. UV-HPLC chromatogram (254 nm) of ^{nat}Ti-DOTA complex. R_t = 3.15 min.

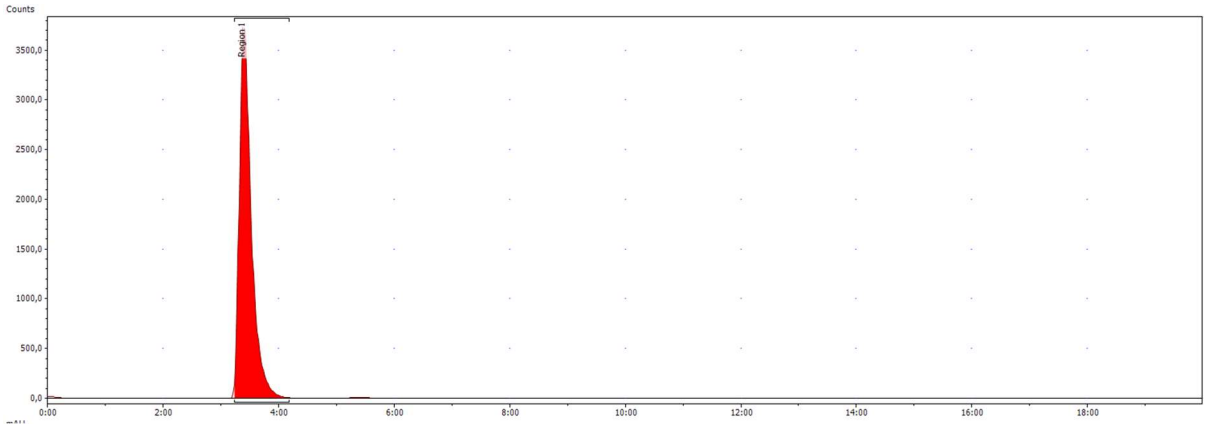

Figure S27. Radio-HPLC (R_t = 3.23 min) chromatogram of [^{45}Ti]Ti-DOTA in the crude product.

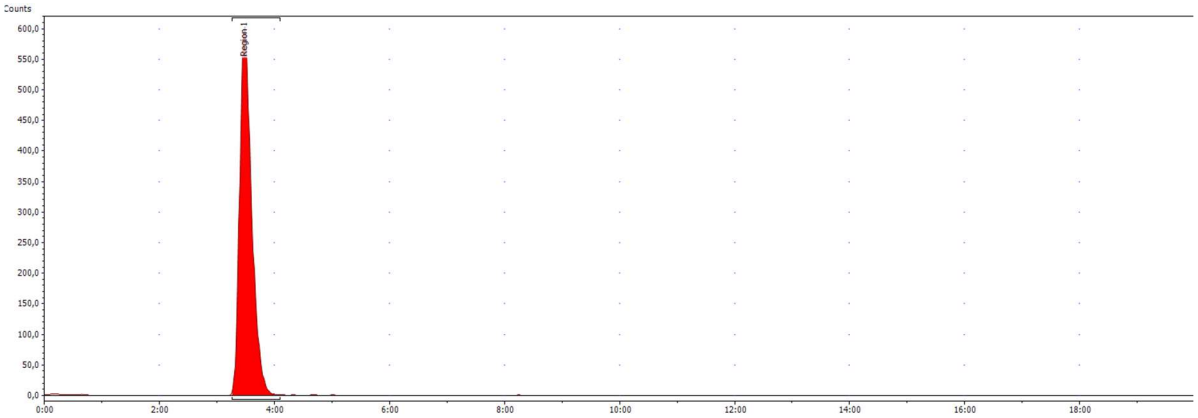

Figure S28. Radio-HPLC (R_t = 3.29 min) chromatogram of [^{45}Ti]Ti-DOTA after purification.

References

1. S. J. C. do Carmo, P. J. H. Scott and F. Alves, *EJNMMI Radiopharm. Chem.*, 2020, **5**, 2.
2. S. Maheshwary, N. Patel, N. Sathyamurthy, A. D. Kulkarni and S. R. Gadre, *J. Phys. Chem. A* 2001, **105**, 10525-10537.
3. M. J. Frisch, G. W. Trucks, H. B. Schlegel, G. E. Scuseria, M. A. Robb, J. R. Cheeseman, G. Scalmani, V. Barone, G. A. Petersson, H. Nakatsuji, X. Li, M. Caricato, A. V. Marenich, J. Bloino, B. G. Janesko, R. Gomperts, B. Mennucci, H. P. Hratchian, J. V. Ortiz, A. F. Izmaylov, J. L. Sonnenberg, Williams, F. Ding, F. Lipparini, F. Egidi, J. Goings, B. Peng, A. Petrone, T. Henderson, D. Ranasinghe, V. G. Zakrzewski, J. Gao, N. Rega, G. Zheng, W. Liang, M. Hada, M. Ehara, K. Toyota, R. Fukuda, J. Hasegawa, M. Ishida, T. Nakajima, Y. Honda, O. Kitao, H. Nakai, T. Vreven, K. Throssell, J. A. Montgomery Jr., J. E. Peralta, F. Ogliaro, M. J. Bearpark, J. J. Heyd, E. N. Brothers, K. N. Kudin, V. N. Staroverov, T. A. Keith, R. Kobayashi, J. Normand, K. Raghavachari, A. P. Rendell, J. C. Burant, S. S. Iyengar, J. Tomasi, M. Cossi, J. M. Millam, M. Klene, C. Adamo, R. Cammi, J. W. Ochterski, R. L. Martin, K. Morokuma, O. Farkas, J. B. Foresman and D. J. Fox, *Journal*, 2016.
4. J. P. Perdew, K. Burke and M. Ernzerhof, *Phys. Rev. Lett.*, 1996, **77**, 3865-3868.
5. J. P. Perdew, K. Burke and M. Ernzerhof, *Phys. Rev. Lett.*, 1997, **78**, 1396-1396.
6. S. Grimme, S. Ehrlich and L. Goerigk, *J. Comput. Chem.*, 2011, **32**, 1456-1465.

7. D. G. A. Smith, L. A. Burns, K. Patkowski and C. D. Sherrill, *J. Phys. Chem. Lett.*, 2016, **7**, 2197-2203.
8. A. V. Marenich, C. J. Cramer and D. G. Truhlar, *J. Phys. Chem. B*, 2009, **113**, 6378-6396.
9. F. Weigend and R. Ahlrichs, *Phys. Chem. Chem. Phys.*, 2005, **7**, 3297-3305.
10. D. Feller, *J. Comput. Chem.*, 1996, **17**, 1571-1586.
11. K. L. Schuchardt, B. T. Didier, T. Elsethagen, L. Sun, V. Gurumoorthi, J. Chase, J. Li and T. L. Windus, *J. Chem. Inf. Model.*, 2007, **47**, 1045-1052.
12. D. Rappoport and F. Furche, *J. Chem. Phys.*, 2010, **133**, 134105.
13. K. A. Peterson, D. Figgen, M. Dolg and H. Stoll, *J. Chem. Phys.*, 2007, **126**, 124101.
14. D. Figgen, K. A. Peterson, M. Dolg and H. Stoll, *J. Chem. Phys.*, 2009, **130**, 164108.
15. Energy-consistent Pseudopotentials of the Stuttgart/Cologne Group, (accessed February 8th, 2024).
16. R. F. Ribeiro, A. V. Marenich, C. J. Cramer and D. G. Truhlar, *J. Phys. Chem. B*, 2011, **115**, 14556-14562.
17. M. Álvarez-Moreno, C. de Graaf, N. López, F. Maseras, J. M. Poblet and C. Bo, *J. Chem. Inf. Model.*, 2015, **55**, 95-103.
18. C. Bo, F. Maseras and N. López, *Nat. Catal.*, 2018, **1**, 809-810.
19. F. Weigend, F. Furche and R. Ahlrichs, *J. Chem. Phys.*, 2003, **119**, 12753-12762.
20. D. Andrae, U. Häußermann, M. Dolg, H. Stoll and H. Preuß, *Theoret. Chim. Acta*, 1990, **77**, 123-141.
21. Z. Meng, Y. He, Y. Wei and Y. Xing, WO2018120923, 2018.
22. D. N. Pandya, N. Bhatt, H. Yuan, C. S. Day, B. M. Ehrmann, M. Wright, U. Bierbach and T. J. Wadas, *Chem. Sci.*, 2017, **8**, 2309-2314.
23. E. P. Meagher and G. A. Lager, *Canad. Mineral.*, 1979, **17**, 77-85.
24. M. Horn, C. F. Schwerdtfeger and E. P. Meagher, *Z. Kristallogr. – Cryst. Mater.*, 1972, **136**, 273-281.
25. J. P. Holland, *Inorg. Chem.*, 2020, **59**, 2070-2082.
26. É. Csajbók, Z. Baranyai, I. Bányai, E. Brücher, R. Király, A. Müller-Fahrnow, J. Platzek, B. Radüchel and M. Schäfer, *Inorg. Chem.*, 2003, **42**, 2342-2349.
27. C. Chen, C. Sommer, H. Thisgaard, V. McKee and C. J. McKenzie, *RSC Advances*, 2022, **12**, 5772-5781.
28. M. Woods, K. M. Payne, E. J. Valente, B. E. Kucera and V. G. Young Jr., *Chem. Eur. J.*, 2019, **25**, 9997-10005.
29. R. Janicki and A. Mondry, *Dalton Trans.*, 2019, **48**, 3380-3391.
30. M. Pniok, V. Kubíček, J. Havlíčková, J. Kotek, A. Sabatie-Gogová, J. Plutnar, S. Huclier-Markai and P. Hermann, *Chem. Eur. J.*, 2014, **20**, 7944-7955.
31. R. Shannon, *Acta Cryst.* , 1976, **A32**, 751-767.